Research Square

Preprints are preliminary reports that have not undergone peer review.
They should not be considered conclusive, used to inform clinical practice,
or referenced by the media as validated information.

Genomic Alterations and Pathologic Responses to Androgen Receptor Pathway Inhibitor Doublets vs. Triplets in the Phase-II Genomic Umbrella Neoadjuvant Study (GUNS) in High-Risk Localized Prostate Cancer

Martin Gleave

m.gleave@ubc.ca

The Vancouver Prostate Centre, Department of Urologic Sciences, University of British Columbia

Joshua Scurll

Department of Urologic Sciences, University of British Columbia https://orcid.org/0009-0007-5855-0127

Himisha Beltran

Dana Farber Cancer Institute and Harvard Medical School https://orcid.org/0000-0003-3259-2226

Eric Belanger

The University of British Columbia

Htoo Zarni Oo

1. Department of Urologic Sciences, University of British Columbia, Vancouver, British Columbia, Canada https://orcid.org/0009-0009-8514-2713

Alexander Wyatt

University of British Columbia

Miles Mannas

University of British Columbia

Peter Black

UBC https://orcid.org/0000-0002-2919-7068

Amina Zoubeidi

University of British Columbia https://orcid.org/0000-0002-0498-142X

Jonathan Ma

Vancouver Prostate Centre

Doron Berlin

University Health Network

Susan Prendeville

University Health Network

Di Jiang
University Health Network
Brant Inman
London Health Sciences Centre https://orcid.org/0000-0002-6060-4485
Brian Chapin
The University of Texas MD Anderson Cancer Center
Todd Morgan
University of Michigan https://orcid.org/0000-0002-1140-0603
Zachery Reichert
University of Michigan https://orcid.org/0000-0003-0356-8796
Adam Kibel
Urology Division, Department of Surgery, Brigham and Women's Hospital, Harvard Medical School
Marc Dall'Era
University of California Davis Comprehensive Cancer Center
Mamta Parikh
University of California Davis Comprehensive Cancer Center
Michael Schweizer
University of Washington
Daniel Lin
Department of Urology, University of Washington
Rodney Breau
University of Ottawa
Lucia Nappi
University of British Columbia
Neil Fleshner
University Health Network

Article

Keywords:

Posted Date: November 5th, 2026

DOI: https://doi.org/10.21203/rs.3.rs-11446928/v1

License: This work is licensed under a Creative Commons Attribution 4.0 International License.
Read Full License

Additional Declarations: Yes there is potential Competing Interest. L.N. has received research support from J&J. M.M. has received honoraria from J&J. A.W. has served on advisory boards and received honoraria from J&J. H.B. has served as a consultant/advisory board member for J&J. P.B. has served as

a member of an advisory board or equivalent for J&J and Roche and has been a member of a Speakers' Bureau for J&J. M.P. has received consulting fees from AstraZeneca and Pfizer. D.M.J. has served as a consultant/advisory board member and has been a member of a Speakers' Bureau for J&J. N.F. has received consulting fees from J&J. M.G. has received research support from J&J and Roche and served as a consultant for J&J. M.D. has served as a member of an advisory board for MDx Health and has received research support from J&J. A.S.K. has served as a consultant/advisory board member for J&J. B.F.C. has received funding for research and for consulting from J&J.

Genomic Alterations and Pathologic Responses to Androgen Receptor Pathway Inhibitor Doublets vs. Triplets in the Phase-II Genomic Umbrella Neoadjuvant Study (GUNS) in High-Risk Localized Prostate Cancer

Martin E. Gleave[1], Joshua M. Scurll[1], Himisha Beltran[2], Eric Belanger[1], Htoo Zarni Oo[1], Alexander W. Wyatt[1], Miles Mannas[1], Peter Black[1], Amina Zoubeidi[1], Jonathan Ma[1], Doron Berlin[3], Susan Prendeville[4], Di Maria Jiang[5], Brant Inman[6], Brian F. Chapin[7], Todd Morgan[8], Zachery R. Reichert[8], Adam S. Kibel[9], Marc Dall'Era[10], Mamta Parikh[10], Michael T. Schweizer[11], Daniel W. Lin[11], Rodney H. Breau[12], Lucia Nappi[1], Neil Fleshner[3]

[1]Vancouver Prostate Centre and Department of Urologic Sciences, University of British Columbia (UBC), Canada; [2]Department of Medical Oncology, Dana-Farber Cancer Institute, Boston, MA, USA; [3]Division of Urology or [4]Department of Laboratory Medicine and Pathobiology, University of Toronto, ON, Canada; [5]Princess Margaret Cancer Centre, University Health Network, Toronto, Canada; [6]London Health Sciences Centre, ON, Canada; [7]MD Anderson Cancer Center, Houston, TX, USA; [8]University of Michigan, Ann Arbor, MI; [9]Department of Urology, Mass General Brigham, Boston, MA; [10]University of California Davis Comprehensive Cancer Center, Sacramento, CA; [11]University of Washington, Seattle, WA; [12]University of Ottawa, ON, Canada.

Funding acknowledgements

Johnson and Johnson (J&J) Pharmaceuticals, Pacific Northwest Prostate Cancer SPORE, PCF Young Investigator Awards to L. Nappi and J.M. Scurll, Terry Fox Research Institute.

Conflicts of interest disclosures statement

L.N. has received research support from J&J. M.M. has received honoraria from J&J. A.W. has served on advisory boards and received honoraria from J&J. H.B. has served as a consultant/advisory board member for J&J. P.B. has served as a member of an advisory board or equivalent for J&J and Roche and has been a member of a Speakers' Bureau for J&J. M.P. has received consulting fees from AstraZeneca and Pfizer. D.M.J. has served as a consultant/advisory board member and has been a member of a Speakers' Bureau for J&J. N.F. has received consulting fees from J&J. M.G. has received research support from J&J and Roche and served as a consultant for J&J. M.D. has served as a member of an advisory board for MDx Health and has received research support from J&J. A.S.K. has served as a consultant/advisory board member for J&J. B.F.C. has received funding for research and for consulting from J&J.

Abstract

GUNS (NCT04812366) is a multi-centre adaptive umbrella phase-II neoadjuvant trial evaluating 24 weeks of biomarker-directed therapy on major pathologic response (MPR) and residual cancer burden (RCB) in men with high-risk localized prostate cancer (HR-LPC) undergoing radical prostatectomy. MPR was defined by ≤ 5 mm longest diameter of the dominant focus or viable RCB ≤ 1 mm^2. Diagnostic biopsies underwent Tempus' 648-gene DNA and whole-transcriptome RNA sequencing (seq). After 8 weeks of androgen receptor pathway inhibitor (ARPI) doublet therapy with androgen deprivation (ADT) plus apalutamide (APA), men were assigned to sub-protocols (SPs) defined by genomic alterations $^{(alt)}$ for an additional 16 weeks of an ARPI-doublet with or without additional therapy. SP-1 randomized men with AR-associated (ETS fusions, *FOXA1*, *SPOP*) or otherwise favourable genomic^{alt} to continue ARPI-doublet (SP-1A) versus triplet therapy that includes another ARPI, abiraterone (SP-1B). SP-2 randomized men with aggressive genomic^{alt} (*RB1*, *PTEN*, *TP53*, *AKT1*) to ARPI-doublet (SP-2A) versus triplet therapy with docetaxel chemotherapy (SP-2B). This analysis reports genomic and pathologic response data for 100 evaluable men enrolled in SP-1 and 48 in SP-2, out of 322 participants enrolled in GUNS. DNA-seq revealed a genomic landscape dominated by ETS gene fusions (41%), *FOXA1* (22%), *TP53* (19%), *PTEN* (15%), and *SPOP* (12%) alterations. In SP-1, MPR was significantly higher in patients treated with triplet (SP-1B) versus doublet (SP-1A) therapy (58% vs. 32%, p = 0.0045) and overall RCB was lower (median 0.73 vs. 2.79 mm^2, p = 0.012). In SP-2, MPR was significantly higher with ARPI-docetaxel triplet (SP-2B) versus doublet (SP-2A) therapy (25% vs. 0%, p = 0.011) with a 4.6-fold reduction in median RCB (7.6 vs. 34.6 mm^2, p = 0.083). Secondary endpoints included ypN1 rates, which trended lower in SP-1B vs. SP-1A (14% vs. 28%) and SP-2B vs. SP-2A (29% vs. 46%). *ERG* fusions tended to have higher RCB, and *SPOP*^{alt} and *FOXA1*^{alt} lower RCB, in SP-1, while PTEN-deficient tumours with a concurrent ETS fusion had the worst pathologic outcomes in SP-2. Transcriptomically, baseline AR signalling was strongly associated with lower RCB following ARPI-only combinations, while immunological signatures were unfavourable, associations that were not seen with docetaxel in SP-2B. In conclusion, genomic-biomarker-directed ARPI-triplet therapies improve MPR rates and RCB distributions in men with HR-LPC, supporting further validation in trials to evolve selection of treatment intensification strategies.

Introduction

Prostate cancer (PC) is a highly heterogeneous disease that progresses slowly in some men, while others develop rapid recurrence and metastases after front-line therapy. Over two thirds of new PC diagnoses in the United States are clinically localized[1], and high-risk localized PC (HR-LPC) accounts for about 15% of these[2]. Typically defined by clinical stage T3 or T4, International Society of Urological Pathology (ISUP) grade group (GG) 4 or 5 (total Gleason score (GS) ≥ 8), or serum prostate-specific antigen (PSA) > 20 ng/mL, HR-LPC has a high rate of recurrence and metastases following radical prostatectomy (RP) or radiotherapy plus androgen deprivation therapy (ADT)[3]. This clinical challenge has spurred interest in combinatorial treatments, including neoadjuvant systemic therapies, to improve local control and metastasis-free survival (MFS).

Initial trials of neoadjuvant ADT before RP for localized PC reported lower positive margin rates but no decrease in PSA recurrence[4,5,6]. Over the past decade, phase-III trials in metastatic castration-sensitive PC (mCSPC) demonstrated improved survival when ADT is combined in doublets with docetaxel or androgen receptor pathway inhibitors (ARPIs) like apalutamide (APA) or abiraterone acetate (ABI)[7,8,9,10,11]. More recently, the PEACE-1[12] and ARASENS[13] trials established the benefit of triplet therapy combining ADT, docetaxel, and an ARPI in men with adverse-risk mCSPC. Despite these improved outcomes, pathologic complete responses (pCR) remained low when similar combinations were evaluated as neoadjuvant therapy in HR-LPC[14,15,16,17,18,19,20], differing from breast or bladder cancer, where pCR rates exceed 30% and are associated with improved outcomes[21,22]. Indeed, major pathologic response (MPR) has been defined and standardized across breast cancer trials[23] and is now accepted as a valid endpoint for approval by regulatory agencies[24]. Phase-II trials of neoadjuvant ARPI doublets reported higher rates of minimal residual disease (MRD) as a measure of residual cancer burden (RCB)[18] and set the stage for the phase-III PROTEUS trial of perioperative luteinizing hormone-releasing hormone agonist/antagonist (LHRHa) + APA or placebo for HR-LPC[25]. PROTEUS reported significantly increased MRD and MFS with the LHRHa-APA doublet, establishing pathologic response (using MRD) as a potential correlate of MFS and laying a foundation for future studies to identify subgroups of HR-LPC that are more or less likely to benefit. Considering the significant genomic heterogeneity of HR-LPC[26,27,28], there is scope to improve outcomes using a more targeted, precision-medicine approach.

Genomic biomarkers offer a precision oncology approach to select patients for specific therapies. For example, targeting homologous recombination repair (HRR)-deficient or PTEN-deficient$^{(def)}$ PC with ARPI-PARP[29,30] or -AKT[31] inhibitor triplet combinations, respectively, improves outcomes in molecularly selected populations in mCSPC. Collectively, these studies support a treatment paradigm in which biologic aggressiveness can be overcome, at least in part, through rational therapeutic intensification beyond ARPI alone. We initiated the Genomic-biomarker-selected Umbrella Neoadjuvant Study (GUNS; NCT04812366) to extend this concept to HR-LPC by prospectively assigning genomically defined high-risk subgroups to ARPI-based regimens matched to their underlying biology. This investigator-initiated, multi-centre phase-II trial has adaptive sub-protocols (SPs) to evaluate pathologic response after combinations of ARPI-doublets vs. triplets guided by specific biomarkers (**Figure 1a**). SP-1 randomizes men with AR-pathway genomic alterations (^{alt})—without co-occurring aggressive tumour suppressor gene (TSG) loss—to an ARPI-doublet (LHRHa/APA) versus ARPI-triplet (LHRHa/APA + ABI), testing the hypothesis that ARPI intensification, in a subgroup potentially more sensitive to ARPI, will increase depth of pathologic response. SP-2 randomizes men with poor-prognosis genomic alterations (*TP53*^{alt}, *PTEN*^{alt} or other AKT-pathway-activating variants, or *RB1*^{alt}) to an ARPI-doublet or a triplet with docetaxel. In this manuscript, we report rates of MPR in 148 participants enrolled in SP-1 and SP-2, along with their baseline diagnostic genomes (648-gene panel) and matching transcriptomes. MPR rates were significantly higher in SP-1 using an ARPI-ABI triplet, and in SP-2B using an ARPI-docetaxel triplet, compared to ARPI-doublets. This work

contributes to understanding treatment response in HR-LPC genotypes and phenotypes, fundamental to evolution of biomarker-targeted treatment strategies.

Methods

Trial Design and Objectives. GUNS (ClinicalTrials.gov: NCT04812366, registered 2021/03/23) is an investigator-initiated, multi-centre, multi-arm adaptive phase-II study in men with HR-LPC who are candidates for RP. The objective is to define the effects of genomic-biomarker-tailored combination therapies on MPR and emergent therapeutic resistance in prostatectomy tissues. Participants were enrolled in a Master Protocol for 8-week treatment with LHRHa plus APA while biopsies were retrieved for genomic sequencing (seq) using the Tempus xT Clinical Laboratory Improvement Amendments (CLIA)-certified assay (see below). Participants with biopsy specimens deemed non-evaluable for genomic testing remained on the Master Protocol for an additional 16 weeks. Following review of evaluable xT genomic reports by a Molecular Tumour Board (MTB), participants were assigned to a specific sub-protocol (SP; Figure 1a) and randomized (if applicable) to a treatment arm within the SP, guided by additional inclusion and exclusion criteria specified in each SP. RP followed 16 weeks of SP treatment. Refer to Supplementary Methods for active sites. J&J provided APA, ABI, and, for SP-3, niraparib. UBC was the lead sponsor. As an investigator-initiated trial, funders reviewed the protocol but did not have a role in design, conduct, analysis, or reporting of results.

The trial was approved by the review board at participating institutions and/or health authorities in Canada and the United States and conducted in accordance with Good Clinical Practice guidelines. All patients provided written informed consent. All authors participated in data interpretation, manuscript drafting, review, and approval before submission.

The primary endpoint is the rate of MPR, as defined below under Pathology Response Assessments, in each SP and arm, when applicable. Secondary endpoints include quantitative RCB determination; correlation of DNA- and RNA-seq data with MPR and RCB; effects on pathologic stage (surgical margins, extracapsular or seminal vesicle extension, lymph-node metastasis); and safety and tolerability of combination regimens in the neoadjuvant setting.

Sub-Protocol Treatments. Men with favourable genomics defined by (i) absence of aggressive genomic^{alt} (*TP53*, *PTEN*, *RB1*, HRR or mismatch repair (MMR) genes) or gain (AKT); (ii) AR-associated alterations (ETS fusion, *FOXA1*, *SPOP*); or (iii) no actionable aberration, were assigned to SP-1 and randomized to SP-1A ARPI-doublet (LHRHa/APA) or SP-1B ARPI-triplet (LHRHa/APA + ABI). Men with unfavourable genomic^{alt} including *TP53*, *PTEN*, *AKT1*, or *RB1* were assigned to SP-2 and randomized to SP-2A ARPI-doublet (LHRHa/ABI) or SP-2B ARPI-chemo triplet (LHRHa/ABI + docetaxel). ABI was used in the SP-2 ARPI-doublet to avoid known drug-drug interactions between APA and docetaxel. See Supplementary Methods for randomization details.

Other GUNS SPs combine an ARPI-doublet with the PARP inhibitor niraparib for HRR defects (SP-3), the PD-L1 inhibitor atezolizumab for tumours with high tumour mutational burden (TMB) and microsatellite instability (SP-4), the EZH2 inhibitor tazemetostat in plasticity-prone PC (SP-5), and the AKT inhibitor capivasertib in PTEN^{def} cancers (SP-6). These SPs are not the subject of this report.

Adverse events (AEs) were assessed according to National Cancer Institute Common Terminology Criteria for Adverse Events, version 5. See Supplementary Methods for additional details.

Patients. Eligible patients had histologically confirmed high-volume HR-LPC defined by any combination of GS 4+3=7 and GS 8 (4+4 or 5+3) in ≥ 6 cores, or ≥ 3 systematic cores with PSA ≥ 20 ng/mL; GS 4+3=7 in ≥ 6 cores and PSA ≥ 20 ng/mL; or ≥ 2 cores with GS ≥ 8, each with ≥ 80% involvement; or GS ≥ 9 in ≥ 1 core. HR-LPC was further divided into four HR tiers, from HR1 (GG4, no features of HR2–4); HR2 (> 2 GG4 biopsy cores or 1–2 GG5 cores; or 1–2 GG4 cores or > 4 GG3 cores, combined with either PSA ≥ 40 ng/mL or stage cT4); HR3 (> 2 GG5 cores; or > 2 GG4 cores or 1–2 GG5 cores, combined with either PSA ≥ 40 ng/mL or stage cT4); HR4 (stage cN1). Participants with ≤ 3 oligometastases by PSMA imaging who were deemed candidates for radical prostatectomy were eligible.

Exclusion criteria included prior systemic or local therapy for localized PC, severe androgen deficiency, or any cancer- or comorbidity-related conditions that precluded candidacy for prostatectomy.

Tissue processing and Immunohistochemistry (IHC). Formalin-fixed paraffin-embedded (FFPE) tissue blocks of prostate needle biopsies were sectioned at 5-µm thickness for haematoxylin and eosin (H&E) staining, PTEN IHC, and genomic sequencing. For sequencing analysis, ten unstained sections and two H&E-stained sections were obtained from the most representative biopsy core, identified based on the highest Gleason score and/or the greatest tumour extent, and sent to Tempus (College of American Pathologists (CAP)-accredited, CLIA-certified sequencing laboratories, Chicago). Freshly sectioned biopsy tissues were assessed in parallel for PTEN expression by IHC (PTEN #9188, Cell Signaling). PTEN expression was quantified based on the percentage of positively stained tumour cells: tumours exhibiting ≤ 10% PTEN-positive cells were classified as negative, 15–45% as low expression, 50–85% as moderate expression, and ≥ 90% as high expression. Additional technical details are described in Supplementary Methods.

DNA and RNA sequencing. FFPE tissue sections, as described above, were sent to Tempus (Chicago, IL) for DNA-seq and RNA-seq using their 648-gene xT panel assay for DNA and the IDT xGen Exome Hybridization Panel, plus additional spike-in probes, for RNA. Tempus provided BAM files aligned to the GRCh37 human reference genome. For RNA-seq, exonic reads per gene were counted using featureCounts[62]. Raw counts were used for differential expression analysis with DESeq2[63] and edgeR[64], while $\log_2$-transformed normalized expression values were used with limma[65]. See Supplementary Methods for normalization details. For xT DNA-seq, genomic variants categorized by Tempus as "variant of unknown significance" (VUS) were excluded (not counted as relevant alterations) unless two or more VUSs were simultaneously identified in the same gene. A copy number (CN) gain reported by Tempus generally meant ≥ +8 copies, and monoallelic deletions were not reported except for loss of heterozygosity of *BRCA1* or *BRCA2*.

TMB harmonization. To compare TMB between GUNS and MSK-IMPACT data, we recalculated TMBs using the Tempus definition based on overlapping target regions between the Tempus xT and MSK-IMPACT panels. For GUNS, we started from Tempus' Molecular Master File (MMF), an intermediate file generated before the final xT report. To first remove potentially false-positive somatic variants arising from cross-contamination in the MMF, we identified identical pairs of variants that appeared as somatic in one patient but germline in another and then removed the somatic ones. We then counted non-synonymous coding variants excluding stop gains (i.e., missense, frameshift, in-frame insertion/deletion, stop-loss, start-codon and exon-loss variants) with ≥ 100× coverage and a variant allele frequency (VAF) > 5% falling within the coding sequences (CDS) shared by the Tempus xT and all MSK-IMPACT panels. TMB was computed as this variant count divided by the total shared CDS length (0.79 Mb).

Pathology Review and Response Assessment. Residual cancer was evaluated on prostatectomy specimens using routine H&E staining. A Pathology Response Committee (E.B., S.P., H.Z.O.), blinded to SP arm assignment, reviewed pathology responses, RCB, and MPR status. All slides were systematically reviewed to identify regions of interest (ROIs) containing viable cancer. In cases demonstrating marked

degenerative or treatment-related changes that limited morphologic assessment on H&E sections, IHC was performed to confirm the presence of residual carcinoma using NKX3.1 and/or cytokeratin AE1/AE3. GUNS initially used pCR as the primary endpoint, but this was amended in 2025 (see Supplementary Methods) because pCR was rare, with an intent to align pathologic response endpoints with the PROTEUS trial. GUNS adopted a composite definition of MPR using ≤ 5 mm long diameter index ROI or quantitative RCB ≤ 1 mm^2, an approach intended to define the area of tumour-cellularity-weighted RCB. MPR can include ypCR, ypT2, ypT3, and ypN1, but requires negative surgical resection margins. RCB was quantified by calculating the index ROI length × width (mm^2) multiplied by the corresponding tumour cellularity (pathologist-estimated percent area covered by cancer cells). ROIs from up to four distinct cancer foci, including lymph-node metastases, were summed when present. MRD was also evaluated using PROTEUS criteria (ypCR or ≤ 5 mm long diameter of the largest ROI, ypT2, and surgical resection margin negative)[25].

Statistical Analysis. The primary endpoint is the rate of MPR in SPs using genomic-biomarker-directed combinatorial regimens. In each trial arm, an MPR rate ≥ 40% would be of interest whereas ≤ 20% would be of insufficient interest. A pre-specified Simon's two-stage design[66] was used with a null hypothesis that the true response rate is ≤ 20%, tested against a one-sided alternative, to impose an interim stopping condition and determine Stage-1 and final sample sizes. In the first stage, 24 patients would be accrued per arm, and an MPR rate ≤ 5/24 would lead to arm closure. Each arm that continued to Stage 2 would accrue an additional 21 patients for a total of 45. Sample sizes were chosen to yield a type-I error rate of 0.05 and power of 0.9 when the true response rate is 40%.

Furthermore, SPs 1 and 2 were each randomized to a doublet-therapy control arm (A) or the triplet-therapy arm (B) and the MPR rate was compared between arms A and B; a statistically significantly greater MPR rate in Arm B vs. Arm A further supports expansion of Arm B. The MPR rate was compared between Arms A and B using either a one-sided two-proportion z test (the one-sided analog of Pearson's chi-squared test), without Yates' continuity correction, if the expected counts for every group in the Arm × Response contingency matrix was ≥ 5 or Fisher's exact test (one-sided) otherwise. Because Stage-2 accrual statistically depended on Stage-1 observations, we performed separate Stage-1 and Stage-2 comparisons of pathologic response in SP-1B vs. SP-1A and summarized overall SP-1 MPR and RCB results by combining one-sided *p* values stagewise using Liptak's weighted inverse-normal method (R function *metaRNASeq::invnorm* with *nrep* = evaluable sample size). Throughout, left-tailed *p* values correspond to the alternative hypothesis that Arm B had favourable response (greater MPR rate or lower RCB) compared to Arm A.

Baseline demographic and clinical characteristics were summarized by descriptive statistics. Univariate pairwise associations between categorical variables were assessed using either Fisher's exact test or a two-proportion z test (equivalent to Pearson's chi-squared test for two-sided alternative hypotheses) following the rule described above. The family-wise error rate was controlled using the Holm method of *p*-value adjustment within the following distinct families of hypothesis tests: (1) MPR or RCB comparisons per SP, (2) secondary endpoints per SP, and (3) clinicopathologic correlates of response per arm. The Benjamini-Hochberg (BH) method of *p*-value adjustment was used to control the false discovery rate (FDR) among genomic associations with baseline clinicopathologic variables and separately among genomic correlates of response per arm. Tests for associations between pre-treatment genomic or clinicopathologic characteristics and pathologic response within each arm were exploratory.

Complete statistical analysis results with details of the tests performed, statistic values, and nominal and adjusted *p* values can be found in Supplementary Tables S3–S17.

Correlative transcriptomic analyses. Exploratory differential gene expression analysis to investigate associations between the baseline (pre-treatment) transcriptomes and pathologic response to treatment

was performed by fitting gene expression to the following statistical model with DESeq2[63], edgeR[64], and limma[65]: `~0 + SP + SP:logRCB + TP`, where `SP` denotes the sub-protocol (treatment arm), `logRCB` = $\log_{10}$(RCB + 1 mm^2), `TP` denotes tumour purity ($0 \le$ `TP` ≤ 1), and `SP:logRCB` denotes the interaction between the `SP` and `logRCB` terms (i.e., their product). Consensus *p* values and log fold-change estimates were derived from the DESeq2, edgeR, and limma results by applying a directional Bonferroni partial-conjunction test to the method-specific raw *p* values [$p = \min\{1, (m - r + 1)p_r\}$, where p_r is the rth-smallest *p* value and r = ceiling(m/2)] and taking the median $\log_2$ fold change across methods. For each contrast of interest (i.e., for the logRCB slope in each SP), genes were ranked for gene set enrichment analysis (GSEA) by the product of their median $\log_2$ fold change and $-\log_{10}(p_r)$, and GSEA was then performed using the "preranked" module in the GSEApy Python module[67].

Results

Patient Cohort. Between September 2021 and July 2026, GUNS enrolled 322 participants across 9 sites in North America. Patient demographics and clinical characteristics are summarized in **Table 1**. Most cancers were GG4 (14.4%) or GG5 (74.4%). To monitor balance across randomized arms, this high-risk (HR) cohort was further subdivided into four HR tiers, from HR1 (lowest risk) to HR4 (highest risk) based on grade, number of cancer-positive biopsy cores, PSA, and clinical node status by imaging at diagnosis (see Methods). Cancer volume at study entry varied significantly given wide ranges in diagnostic PSA and HR grouping, but these were balanced between arms (**Table 1**). Reflecting the high-risk nature of our cohort, where recorded, intraductal carcinoma (IDC) was noted in 37% of biopsy reports and non-IDC cribriform morphology in 48% (**Table 1**), with 24% having both. Patients were assigned to SPs based on genomic biomarkers in diagnostic biopsies sequenced by Tempus xT (**Figure 1a**).

Genomic Landscape of HR-LPC in GUNS. Genomic alterations in GUNS were broadly consistent with other Western PC cohorts, with AR-regulated ETS oncogene fusions (41% any ETS, 35% *ERG*), *FOXA1*^{alt} (22%), *TP53*^{alt} (19%), *PTEN*^{alt} (15%), and *SPOP*^{alt} (12%) the most frequent (**Figure 1b**). While *ERG* fusions were common in both SP-1 and SP-2 (34% SP-1 vs. 43% SP-2, $p = 0.29$), *SPOP*^{alt} and *FOXA1*^{alt} were enriched in SP-1 compared to SP-2 (**Figure 1b**), consistent with known tendencies for *PTEN*^{alt} or *TP53*^{alt} to co-occur with *ERG* fusions[32,33,34,35] and for *SPOP*-mutant tumours to be de-enriched for *TP53*^{alt}, *PTEN*^{alt}, and *RB1*^{alt} (ref. 36). These data also suggest that *FOXA1*^{alt} tends not to co-occur with those aggressive tumour suppressor gene losses in treatment-naive HR-LPC. Importantly, the three common AR-related genotypes (ETS fusion, *SPOP*^{alt}, and *FOXA1*^{alt}) covered 78% of SP-1 patients (and 71% of the whole cohort). In SP-2, which focused specifically on genotypes associated with aggressive disease and ARPI resistance, *TP53*^{alt} was most common (57%), followed by *PTEN*^{alt} (51%) (**Figure 1b**). Other PI3K/AKT-pathway-activating mutations and *RB1*^{alt} occurred at low frequencies in SP-2 (*AKT1*: 2/49; *PIK3CA*: 1/49; *RB1*: 3/49). Monoallelic deletions were not reported by Tempus xT. Within each SP, the frequent alterations were balanced between arms (**Supplementary Figure S1a**).

Only genomic alterations were considered for assignment to SP-2, but PTEN IHC was assessed where available. While 69% of genomically *PTEN*^{alt}, and 13/16 (81%) of biallelic *PTEN*-deleted, cases with available PTEN IHC data were considered PTEN$^{IHC\text{-}negative}$ (positive staining in ≤ 10% of cancer cells), 13% of tumours without a reported genomic *PTEN*^{alt} were also PTEN$^{IHC\text{-}negative}$, including 12/79 (15%) SP-1 cases (**Figure 1c** and **Supplementary Figure S1b**). Discordant genomic and IHC data for PTEN could be due to genomic alterations, especially large structural rearrangements, being missed/unreported by Tempus xT, or they could reflect other mechanisms of PTEN loss, such as epigenetic silencing or post-transcriptional/-translational regulation, or intratumour heterogeneity.

Across the whole GUNS cohort, PTEN loss as measured by IHC was strongly correlated with observation of IDC on biopsy (not necessarily in the same biopsy core assessed for PTEN IHC or Tempus xT; **Figure 1d**), consistent with the enrichment of IDC in SP-2. Even tumours with heterogeneous PTEN IHC displayed an almost two-fold increase in the rate of IDC compared to tumours with ≥ 90% PTEN positivity, suggesting that IDC developed from PTEN-negative subclones in heterogeneous tumours. This association was more specific for IDC than for general cribriform pattern (**Supplementary Figure S1c**) and was more pronounced than for *PTEN*^{alt} identified by Tempus xT (**Supplementary Figure S1d**). *TP53*^{alt}, on the other hand, correlated with any IDC or cribriform pattern on biopsy (**Figure 1e** and **Supplementary Figure S1e**). Interestingly, however, IDC was especially likely in tumours that exhibited both *TP53*^{alt} and an ETS fusion (**Figure 1f**) even though ETS fusions were not independently significantly associated with IDC or cribriform histology (**Supplementary Figure S1f**). These observations support prior studies linking IDC to PTEN loss, ERG expression, and *TP53* mutations[37,38] and additionally reveal possible cooperation between ETS transcription factors and TSG loss in driving aggressive pathology.

Overall tumour mutational burdens (TMBs) did not differ between SP-1 and SP-2 and were almost all < 10 mut/Mb in these two SPs (**Figure 1g**), as high TMB (≥ 10 mut/Mb) was a biomarker for SP-4 (ARPI + anti-PD-L1 immunotherapy). Comparison of TMBs across GUNS to publicly available MSK-IMPACT data[39], after harmonizing TMB calculations (see Methods), showed that TMBs in GUNS matched HR-LPC TMBs in the MSK-IMPACT cohort and, moreover, that HR-LPC TMBs were more similar to TMBs in mCSPC and even metastatic castration-resistant PC (mCRPC) than to TMBs in intermediate-risk localized PC (**Figure 1h**).

Major pathologic responses in SP-1 were higher with ARPI-triplet compared to doublet therapy. SP-1 randomized participants with only AR-associated (*FOXA1*^{alt}, *SPOP*^{alt}, ETS fusion) or otherwise favourable genomic alterations to an ARPI doublet (SP-1A) or triplet with ABI (SP-1B) to test whether ARPI intensification increases depth of pathologic response. Stage 1 evaluated 24 participants per SP-1 arm; both arms had > 5 MPRs, but MPRs were significantly more frequent in SP-1B than 1A (15/24 (63%) vs. 8/24 (33%), $p = 0.022$, **Supplementary Figure S2a**), supporting continuation of SP-1 to Stage 2. Overall, SP-1 enrolled a total of 100 participants who underwent prostatectomy, and the GUNS composite MPR rate remained significantly greater in SP-1B than 1A (29/50 (58%) vs. 16/50 (32%), stagewise-combined $p = 0.0045$, Holm-adjusted $p = 0.013$, odds ratio (OR) = 2.90, OR 95% confidence interval (CI) = [1.20, 7.22]; **Figure 2a**). There were two pCRs in each SP-1 arm. PROTEUS-trial-defined MRD criteria were more stringent and accounted for less than a third of patients on SP-1, with no significant difference between SP-1A and SP-1B (**Supplementary Figure S2b**). **Supplementary Table S1** lists MPR cases in GUNS that did not meet PROTEUS criteria. RCB was evaluated as a broader measure of depth of pathologic response and there was a consistent shift to lower RCB with ARPI-triplet intensification in SP-1B across the full RCB range (median 0.73 vs. 2.79 mm^2, mean 12.3 vs. 37.6 mm^2; stagewise-combined Wilcoxon rank-sum $p = 0.012$, Holm-adjusted $p = 0.024$; **Figure 2b**).

MPR rates in SP-2 were higher with an ARPI-docetaxel triplet than an ARPI-doublet. SP-2 tested the hypothesis that an ARPI-docetaxel triplet would increase depth of pathologic response compared to an ARPI-doublet in cancers with aggressive genomic^{alt} (*TP53*, *PTEN*, *RB1*, *AKT1*). In Stage 1, 49 men with these genomic^{alt} were randomized and well balanced across HR groups (**Table 1**), of whom 48 were evaluable for pathologic endpoints. Compared to the overall cohort and to SP-1, however, SP-2 had higher proportions of cases with IDC/cribriform pattern, and cN1, likely reflecting aggressive genomics and biology.

MPR was significantly higher in the ARPI-docetaxel triplet arm SP-2B compared to the ARPI-doublet arm SP-2A (6/24 vs. 0/24, OR = Inf, OR 95% CI = [1.34, Inf), $p = 0.011$, Holm-adjusted $p = 0.033$; **Figure 2c**); there was also one pCR in SP-2B. The MRD rate using PROTEUS criteria was 4/24 vs. 0/24 ($p = 0.055$, Holm-adjusted $p = 0.109$; **Supplementary Figure S2c**), the difference due to one patient having an ROI of 9.3 ×

0.7 mm with 1% tumour cellularity, and another having a 1.8-mm organ-confined prostatic index ROI with a 4-mm sparsely cellular lymph node deposit. RCB also trended lower in SP-2B than in SP-2A (Wilcoxon rank-sum $p = 0.083$, Holm-adjusted $p = 0.109$; **Figure 2d**), with seven SP-2B patients having lower RCB than the minimum RCB achieved in SP-2A (2.05 mm^2) and a 4.6-fold reduction in median RCB (7.6 vs. 34.6 mm^2). The magnitude of effect is consistent with the significant improvement in the MPR endpoint and supports a shift towards lower RCB with ARPI-docetaxel triplet therapy in tumours characterized by aggressive genomic^{alt}. SP-2B has been expanded to Stage 2, which is enrolling at the time of this report.

Comparison of MPR and RCB in SP-1 and SP-2 illustrates higher MPR and lower RCB in SP-1 vs. SP-2, with ARPI-ABI triplets in SP-1B yielding the lowest RCB and highest MPR rate (**Supplementary Figure S2d**). There was a consistent shift to lower RCB with ARPI-triplet intensification in both SP-1 and SP-2, with the magnitude and statistical strength of this effect greater in SP-1 than SP-2. **Figure 2e** illustrates representative examples of RCB and MPR that highlight the varying tumour and stromal cellularity in SP-1 and SP-2 cases.

Secondary Endpoints. Pre-surgery nadir serum PSA levels did not significantly differ between SP-1B and SP-1A (**Figure 3a**); 38/50 (76%) SP-1B vs. 33/49 (67%) SP-1A patients had PSA nadir levels ≤ 0.03 ng/mL or otherwise undetected (if the limit of detection was > 0.03 ng/mL). Pathologic T (ypT) stages also did not significantly differ (**Figure 3b**) and positive margin rates were similarly low in SP-1B and SP-1A (6/50 (12%) vs. 8/50 (16%); **Figure 3c**), while ypN1 was half as frequent in SP-1B as in SP-1A (7/50 (14%) vs. 14/50 (28%); $p = 0.043$, Holm-adjusted $p = 0.171$; **Figure 3d**). In SP-2, pre-surgery nadir PSA levels were similar in both arms (**Figure 3e**; ≤ 0.03 ng/mL or otherwise undetected in 16/24 (67%) SP-2B vs. 14/23 (61%) SP-2A), but SP-2B was significantly enriched for ypCR or ypT2 (9/24) compared to SP-2A, where 22/24 cases were ypT3 ($p = 0.0082$, Holm-adjusted $p = 0.033$; **Figure 3f**). Additionally, positive margin and ypN1 rates were both reduced, albeit not statistically significantly, in SP-2B compared to SP-2A (2/24 vs. 6/24, $p = 0.12$, Holm-adjusted $p = 0.35$; and 7/24 vs. 11/24, $p = 0.12$, Holm-adjusted $p = 0.35$, respectively; **Figure 3g–h**).

Treatment-emergent serious adverse events (TE-SAEs). TE-SAEs were uncommon in SP-1 but occurred more frequently in SP-2B, primarily reflecting expected chemotherapy-related toxicity (**Supplementary Table S2**). Febrile neutropenia was the most frequent serious adverse event and occurred exclusively in patients receiving docetaxel. No unexpected safety signals were observed, and the spectrum of SAEs was consistent with the known safety profiles of ARPI and docetaxel. One participant in SP-2B had febrile neutropenia and a stroke while on chemotherapy and became a non-surgical candidate. Another participant developed a headache during the Master Protocol that resolved after an APA dose reduction. After assignment to SP-1B, Grade-2 headache with Grade-3 arthralgia occurred that led to treatment discontinuation and trial withdrawal.

Canonical AR signalling was associated with low, and *ERG* fusions with high, RCB after ARPI. To identify potential biomarkers of response to ARPI-doublet therapy in SP-1A and SP-2A or ARPI-triplet therapy in SP-1B, we tested for associations between pathologic response and baseline clinicopathologic, genomic, and transcriptomic characteristics of cancers at diagnosis (**Supplementary Tables S10–S15)**. Within SP-1A, *ERG* fusions were significantly associated with higher RCB (**Figure 4a**) and more common in non-MPR than MPR cases (**Supplementary Figure S3a**). There were two cases in SP-1A with other ETS fusions and both were non-MPR with high RCB (**Figure 4b**). Conversely, *SPOP*^{alt} and *FOXA1*^{alt} were associated with lower RCB (**Figure 4c–d**) and more common in MPR than non-MPR cases (**Supplementary Figure S3b–c**). Additionally, the 11 PTEN$^{IHC\text{-}negative}$ cases in SP-1A (with no genomic *PTEN*^{alt} by xT) were associated with greater RCB (**Figure 4e**) and no MPR. With intensified ARPI in SP-1B, the unfavourable trends for *ERG*/ETS fusions were weakened (**Figure 4f–g** and **Supplementary Figure S3d**), the negative association between *SPOP*^{alt} and RCB strengthened (**Figure 4h** and **Supplementary Figure S3e**), and the associations between *FOXA1*^{alt} or PTEN

IHC and RCB were effectively lost (**Figure 4i–j** and **Supplementary Figure S3f**). These trend shifts from SP-1A to SP-1B were driven by broad reductions in RCB but with variable magnitudes across different genomic and PTEN-IHC groups.

In SP-2A, as already emphasized, there were no MPR cases, compared with 32% in SP-1A (**Figure 2**), underscoring *TP53*^{alt} and *PTEN*^{alt} as unfavourable, though the switch in ARPI from APA to ABI at Week 8 in SP-2A versus continuation of APA alone in SP-1A may be a confounding factor. *TP53*^{alt} and *PTEN*^{alt} did not significantly differ in terms of RCB (**Supplementary Figure S3g–h**), but tumours in which they co-occurred had higher RCB (**Supplementary Figure S3i**). The most significant genomic correlate of RCB in SP-2A was the combination of PTEN^{def} with an ETS fusion (**Figure 4k**); interestingly, this was more significant than the combination of *TP53*^{alt} with an ETS fusion (**Figure 4l**). There were only two cases of *FOXA1*^{alt} in SP-2A and both were associated with favourable response (**Supplementary Figure S3j**), while there were no *SPOP*^{alt} cases in SP-2A. These results demonstrate a continued tendency for ETS fusions to be unfavourable for ARPI, and *FOXA1*^{alt} favourable albeit uncommon, in the context of aggressive genomic^{alt}.

At the transcriptomic level, we assessed the association between gene expression and RCB via differential gene expression analysis with $\log_{10}$(RCB + 1 mm^2), SP, and tumour purity as the independent predictor variables (see Methods). Gene set enrichment analysis (GSEA) then revealed that the level of AR signalling in the diagnostic biopsy, as measured by signature gene sets, consistently and strongly correlated with lower RCB across all three ARPI-only doublet- and triplet-therapy arms (SP-1A, -1B, and -2A) (**Figure 4m–o** and **Supplementary Figure S4**). As indicators of response, the MSigDB Hallmark "androgen response" and CRPC-AR Tang 2022 gene sets outperformed other AR signature gene sets (Spratt 2020, Hieronymus 2006, and Sharma 2013) in all three arms. Conversely, expression of immunological gene sets before treatment was generally associated with higher RCB after treatment in all three ARPI-only arms (**Figure 4m–o**). Notably, although signatures of immunosuppressive cells (e.g., myeloid-derived suppressor cells and regulatory T cells) trended in this same higher-RCB direction, immune-promoting signatures were more significant in this analysis. For instance, Hallmark "allograft rejection" (indicative of an immune response against non-self or neoantigens), interferon signalling, and type-I T-helper cell gene sets were especially prominent in their consistent associations with RCB, with the latter the only gene set to achieve a statistically significant positive association with RCB in all three of SP-1A, SP-1B, and SP-2A. Collectively, these genomic and transcriptomic analyses suggest that baseline AR signalling, and genomic^{alt} linked to enhanced AR signalling (*SPOP*^{alt} and *FOXA1*^{alt}), are the strongest indicators of pathologic response to ARPI and that, counterintuitively, immunological pre-enrichment of prostate tumours is associated with higher RCB. The comparatively unfavourable nature of ETS fusions despite their regulation by AR is perhaps because they drive oncogenic transcriptional programmes very distinct from canonical AR signalling[40,41].

Luminal and basal subtypes have been associated with PC prognosis and response to ADT[42,43], so we included gene sets representing the luminal-like (PCS1, PCS2) and basal-like (PCS3) PC subtypes identified by You *et al*.[42] in our analysis. The gene set defining the aggressive PCS1 subtype, as well as proliferation-related gene sets linked to the PCS1 phenotype, were the gene sets besides AR signalling most significantly associated with lower RCB in SP-1A (**Figure 4m**). The same PCS1 trend was close to significance in SP-2A but far from significance in SP-1B. PCS1 is most like Luminal-B (LumB) in the PAM50 system[44] and has the worst overall prognosis of the three PCS subtypes[42,44]. Our analysis suggests that, consistent with LumB being the PAM50 subtype to benefit most from adjuvant ADT despite otherwise having the worst prognosis[43], PCS1-like HR-LPC benefits more than PCS2 or PCS3 from neoadjuvant ARPI. However, the diminishment of this and other transcriptomic/genomic RCB associations in SP-1B suggests that an ARPI-triplet with ADT, APA, and ABI may overcome some intrinsic resistance to an ARPI doublet.

AR signalling was not predictive of response to the ARPI-docetaxel triplet therapy in SP-2B. To determine how molecular correlates and possible biomarkers of pathologic response change with an ARPI-docetaxel triplet, we repeated the above correlative analyses for SP-2B (**Supplementary Tables S16–S17**). ETS fusions continued to show an unfavourable trend (**Figure 5a–b**), with the combination of an ETS fusion with PTEN^{def} once again being the most significant genomic correlate of higher RCB (**Figure 5c**), more so than the combination of an ETS fusion with *TP53*^{alt} (**Figure 5d**). *FOXA1*^{alt} (**Figure 5e**) and, to a lesser degree, *SPOP*^{alt} (**Figure 5f**) maintained favourable trends, but both were uncommon alterations in SP-2B. However, no genomic associations with pathologic response achieved statistical significance, and trends were substantially weaker than in the other SPs. Moreover, there was no meaningful difference between *PTEN*^{alt} and *TP53*^{alt} in terms of RCB (**Figure 5g–h**). At the transcriptomic level, a signature of *ERG* fusion was positively (unfavourably) associated with RCB and was the only significant gene set in either direction (**Figure 5i**). Notably, AR-signalling signatures were no longer significantly associated with lower RCB and, moreover, were not even among the top-ranked gene sets (though their correlation with RCB was still negative); the Hallmark G2M-checkpoint signature was instead the top-ranked association with favourable response to the ARPI-docetaxel triplet (**Figure 5i**), consistent with docetaxel having stronger effects on more-proliferative cells. These results suggest that addition of docetaxel to an ARPI doublet for genomically aggressive HR-LPC overcomes the necessity for a high level of baseline AR signalling to achieve the best responses. Nevertheless, the low rate of MPR and greater RCB in SP-2B compared to SP-1 highlight that addition of docetaxel to ARPI does not completely overcome the therapy resistance imparted by aggressive genomics. Finally, in contrast to the favourable association between PTEN-inactivity transcriptomic signatures and survival benefit from docetaxel found by Grist *et al*. in the STAMPEDE trials[45], we did not identify a significant association between transcriptomic signatures of PTEN loss and RCB in SP-2B. This is possibly because SP-2 was already selected for the aggressive genotypes most likely to benefit from docetaxel and is therefore not inconsistent with the STAMPEDE docetaxel subgroup analysis.

Discussion

GUNS is a multi-arm umbrella phase-II study with an adaptive design for men with HR-LPC using a neoadjuvant model to evaluate pathologic responses as a surrogate of contextual lethality after biomarker-directed ARPI-doublet and triplet regimens. GUNS enrolled candidates for prostatectomy with high-volume HR-LPC, excluding low-volume GG4 cancers to ensure that evaluation of depth of pathologic response is less confounded by lower-volume disease at baseline. High-volume, high-grade cancer in diagnostic needle biopsies also ensures sufficient tumour cellularity for DNA/RNA extraction using the CLIA-certified Tempus xT test. Higher DNA tumour content enhances detection of alterations, such as copy number deletions common in PC, which is often challenged by low tumour cellularity from stromal infiltrative disease. Tempus xT requires ≥ 20% tumour cellularity and 100 ng input DNA[46]; insufficient quantity or quality of DNA for xT is reported by Tempus as “quantity or quality not sufficient (QNS)”. In GUNS, 13% of samples were QNS and hence unevaluable for SP assignment, similar to sequencing failure rates in other studies in metastatic PC.

HR-LPC is clinically and, as demonstrated by our TMB comparison with the MSK-IMPACT cohort, genomically aggressive[28], with high recurrence rates after surgery alone, and hence requires multimodal intervention to treat both local and potential subclinical metastatic disease. Early studies of neoadjuvant ADT prior to surgery did not enrich for HR-LPC and failed to detect reduced recurrence rates[4,5,6]. The Alliance 90203 trial[19] evaluated 6 months of neoadjuvant ADT plus docetaxel in HR-LPC, but the primary endpoint of biochemical recurrence was confounded by early salvage therapies. This trial began prior to

approval of second-generation ARPI, and pCR/MRD rates were low. Indeed, pCR rates were also low (< 8%) in localized PC treated with neoadjuvant LHRHa doublets of ARPI[14,15,16,47,48] or docetaxel[19,49,50], despite improved survival with these combinations in metastatic PC[7,8,9,10,11]. In contrast, neoadjuvant therapies in breast or bladder cancer induce high pCR rates (> 30%) and associate with improved outcomes[22,51,52,53]. Contemporary neoadjuvant trial designs with rich translational correlates, such as I-SPY 2 in breast cancer[54,55] and GUNS in prostate cancer, provide robust platforms for analysing novel agents and identify new approaches to overcome *de-novo* resistance to endocrine therapy. In breast cancer patients who do not achieve an MPR, RCB (a measure of size combined with cellularity) is prognostic, and might identify patients who could benefit from further adjuvant therapy[53]; this remains to be established in PC.

Recent studies using ARPI doublets in the neoadjuvant setting for HR-LPC helped refine MRD as a measure of therapeutic response[56], which, along with stringent inclusion criteria for high-risk PC and use of PSMA-PET measures of MFS, helped evolve the design of the PROTEUS trial[25]. PROTEUS randomized more than 2,100 men with HR-LPC to perioperative ADT with or without APA and demonstrated significant improvements in both MFS and MRD. PROTEUS is the first study to show that MRD rates are concordant with MFS in the context of neoadjuvant therapy and prostatectomy. The use of MFS and MRD as surrogates for clinical benefit sets the stage to use pathologic response to characterize synthetic lethality using genomic-biomarker-guided combinations in GUNS.

The significant genomic heterogeneity in advanced PC results in subgroups that respond variably to ARPI doublet therapy and supports a targeted, precision-oncology approach for treatment intensification with triplet therapies. GUNS builds upon the PROTEUS paradigm to characterize this important population. While PROTEUS compared an ADT-singlet to an ARPI-doublet, GUNS tests whether further intensification with biomarker-directed ARPI-triplets deepens pathologic responses within biologically defined genomic subgroups. Genomic alterations that rewire the AR transcriptional programme—ETS fusions, *FOXA1*^{alt}, and *SPOP*^{alt}—comprise the largest genomic subgroup of HR-LPC. These early clonal driver events are biologically linked to AR-dependent prostate epithelial identity and tend to define distinct molecular subclasses. *SPOP*^{alt} impairs ubiquitin-mediated degradation of AR/chromatin regulatory proteins and is associated with an AR-responsive, ETS-negative subtype. The pioneer transcription factor FOXA1 opens compacted chromatin to guide AR binding across the genome and prostate luminal epithelial differentiation. *FOXA1*^{alt} redirects AR signalling towards oncogenic transcriptional programmes and, as with *SPOP*^{alt}, tumours remain highly AR-dependent. *TMPRSS2-ERG* gene fusion causes aberrant androgen-driven ERG overexpression that promotes invasion, plasticity, and altered differentiation.

SP-1 randomized 100 evaluable men, most of whom had cancers with these AR-associated genomic alterations, to an ARPI-doublet or -triplet with ABI. MPR was significantly higher with ARPI-triplet compared to doublet therapy, and there was a statistically significant shift towards lower RCB in SP-1B. Prior studies in non-selected populations evaluating addition of ABI to an ARPI doublet did not demonstrate improved outcomes[57,58], implying MPR is not an indicator of clinical benefit; conversely, this improved MPR may underline the importance of biomarker selection in refining outcomes. The lack of signal by triplet intensification in a non-selected study may reflect failure to detect a benefit that occurs in a smaller subgroup of that population. ETS fusions and PTEN$^{IHC\text{-}negative}$ status were more common in non-MPR cases, consistent with biology of ERG and AKT oncogenic signalling pathways that support AR independence. While tumours with *PTEN*^{alt} were assigned to SP-2, assessment of PTEN$^{IHC\text{-}negative}$ status was not routinely performed until SP-1 completed accrual and SP-6 (ARPI + capivasertib) opened in early 2026.

The second most common genomic subgroup in GUNS comprises tumours with loss-of-function aberrations involving *TP53*, *PTEN*, or *RB1*, TSGs that regulate critical cellular processes including DNA

damage response, cell-cycle control, lineage fidelity, and PI3K/AKT signalling. While each alteration individually associates with adverse outcomes, co-loss of *TP53*, *PTEN*, and/or *RB1* has synergistic biologic effects that promote aggressive clinical behaviour and treatment resistance[59,60]. More recent molecular analyses from STAMPEDE and related datasets[45] have similarly identified transcriptional programmes associated with aggressive disease biology, including interferon-response and lineage plasticity signatures that correlate with poorer clinical outcomes despite contemporary systemic therapy. Together, these data associate TSG-loss tumours with progressively less dependence on canonical AR signalling and support non-AR-directed treatment intensification. In patients with adverse-risk metastatic CSPC, the addition of an ARPI to an ADT-docetaxel doublet significantly improved overall survival[12,13]. Consistent with these studies, HR-LPC patients with these aggressive TSG-loss genotypes treated with an ARPI-docetaxel triplet in SP-2B had higher MPR rates. Notably, however, SP-2A and SP-2B cancers had significantly lower MPR rates (0 vs. 25%) and higher median RCB (34.6 vs. 7.6 mm^2) than SP-1A and 1B cancers (32% vs. 58%; 2.8 vs. 0.73 mm^2), findings consistent with a growing body of evidence that loss of *TP53*, *PTEN*, or *RB1* associates with more rapid progression to castration resistance, and support ARPI-docetaxel intensification to partially overcome the adverse biology associated with TSG-loss tumours.

Correlative genomic analyses further support biologically distinct mechanisms of therapeutic sensitivity and resistance. *SPOP*^{alt} tumours were enriched among patients achieving MPR, consistent with prior observations that *SPOP*^{alt} defines an AR-dependent molecular subtype characterized by heightened sensitivity to ARPI. In contrast, ETS fusions were consistently associated with greater RCB across SPs 1 and 2. This observation extends previous reports of ERG expression/fusion associating with inferior response to ADT/ARPI in both localized and metastatic PC[17,61] to doublet- and triplet-therapy regimens in biomarker-stratified patient groups. Moreover, ETS fusions were associated with unfavourable cribriform/IDC pathology in tumours co-harbouring *TP53*^{alt}. *TP53*^{alt} or PTEN^{def} individually associated with IDC; however, the relationship with *TP53*^{alt} was strengthened with concurrent ETS fusion events, suggesting cooperation in driving aggressive histologic phenotypes. Together, these findings support a model in which ETS activation promotes relative AR independence, both independently of and in concert with aggressive tumour suppressor loss, thereby limiting the depth of response achievable with ARPI alone.

While GUNS is signal-finding and not intended to change current clinical practice, the observed magnitudes of difference in MPR warrant assessment against longer-term clinical outcomes. The most notable finding was the marked shift in the entire distribution of RCB towards low-burden states with triplet intensification. This effect was most pronounced in SP-1, where AR-associated tumours demonstrated remarkable sensitivity to an intensified ARPI-triplet, but tumours characterized by TSG loss in SP-2 still exhibited modest but statistically significant improvement in MPR with an ARPI-docetaxel triplet. The observed reduction in median RCB and enrichment of low-burden disease states are biologically consistent with deeper elimination of treatment-sensitive tumour clones and may ultimately translate into improved long-term outcomes.

PROTEUS employed a ≤ 5 mm linear-length MRD endpoint, a binary endpoint that may not fully capture the spectrum of RCB following treatment. Although MRD remains clinically intuitive, a 5-mm linear length alone does not account for differences in area or tumour cellularity, which can vary greatly post-treatment, and hence does not fully discriminate patients with markedly different amounts of viable RCB. GUNS adopted a quantitative framework for RCB, incorporating both the spatial extent of residual disease and the marked hypocellularity that can occur following neoadjuvant ARPI. The substantial shift in RCB distributions observed with triplet intensification in both SP-1 and SP-2 suggests that RCB may provide additional biologic resolution beyond linear-length MRD alone. Although the GUNS area-based RCB cannot be directly converted to a 3-dimensional tumour volume without assumptions regarding tumour depth, it provides a more granular assessment of treatment response and may distinguish biologically

meaningful differences among tumours that would otherwise fall within the same binary MRD category. Accordingly, GUNS complements the PROTEUS framework by extending pathologic response assessment from a principally one-dimensional threshold to a quantitative estimate of viable RCB. A limitation of the current study is that RCB categories are exploratory and not validated as surrogate endpoints in HR-LPC. Future correlation of RCB with tumour cellularity as estimated by DNA[49], MFS, and overall survival with PROTEUS will further evolve quantitative measures of MRD as a surrogate of MFS.

More broadly, GUNS provides a proof of concept for a genomically segmented neoadjuvant strategy in HR-LPC. Rather than treating HR-LPC as a single clinical entity, GUNS prospectively matched biologically distinct molecular subgroups to rational ARPI-based triplet regimens. The differential response patterns observed across genomic cohorts suggest that therapeutic vulnerabilities differ substantially according to underlying disease biology and support further development of precision oncology approaches in HR-LPC, which are ongoing in SPs using ARPI-triplets with PARP, AKT, and PD-L1 inhibitors. Future analyses integrating MPR, continuous RCB distributions, tumour-content DNA, and genomic subtypes will be critical to determine whether depth of pathologic response can serve as a surrogate marker of synthetic lethality and clinical benefit in biomarker-selected populations. Future studies will also leverage pre- and post-treatment tissue specimens to understand how tumour genomics and heterogeneity influence treatment responses, early adaptation, and resistance pathways.

Characteristic	Overall	1A	1B	2A	2B
n	322	52	50	24	25
Age, years (mean (SD))	65.11 (7.21)	66.42 (7.31)	66.12 (6.44)	64.21 (8.35)	63.24 (6.66)
Race (%)					
Asian	42 (13.0)	10 (19.2)	6 (12.0)	1 (4.2)	1 (4.0)
Black or African American	19 (5.9)	2 (3.8)	2 (4.0)	1 (4.2)	2 (8.0)
White	259 (80.4)	39 (75.0)	42 (84.0)	22 (91.7)	22 (88.0)
Unknown or not reported	2 (0.6)	1 (1.9)	0 (0.0)	0 (0.0)	0 (0.0)
PSA, ng/mL (%)					
< 10	125 (38.8)	18 (34.6)	21 (42.0)	6 (25.0)	9 (36.0)
10 ≤ PSA < 20	90 (28.0)	17 (32.7)	17 (34.0)	9 (37.5)	6 (24.0)
20 ≤ PSA < 40	58 (18.0)	10 (19.2)	7 (14.0)	5 (20.8)	3 (12.0)
40 ≤ PSA < 80	43 (13.4)	6 (11.5)	4 (8.0)	4 (16.7)	5 (20.0)
≥ 80	6 (1.9)	1 (1.9)	1 (2.0)	0 (0.0)	2 (8.0)
Grade group (%)					
2	6 (1.9)	0 (0.0)	2 (4.0)	1 (4.2)	1 (4.0)
3	30 (9.4)	6 (11.5)	2 (4.0)	3 (12.5)	4 (16.0)
4	46 (14.4)	9 (17.3)	5 (10.0)	3 (12.5)	3 (12.0)
5	238 (74.4)	37 (71.2)	41 (82.0)	17 (70.8)	17 (68.0)
IDC = Yes (%)	74 (36.8)	15 (28.8)	16 (32.7)	15 (62.5)	9 (37.5)
Cribriform = Yes (%)	96 (48.2)	23 (44.2)	17 (35.4)	13 (54.2)	16 (66.7)
cT stage (%)					
T1	54 (16.9)	6 (11.5)	15 (30.0)	2 (8.3)	4 (16.0)
T2	161 (50.3)	29 (55.8)	22 (44.0)	14 (58.3)	13 (52.0)
T3	97 (30.3)	16 (30.8)	13 (26.0)	8 (33.3)	8 (32.0)
T4	2 (0.6)	0 (0.0)	0 (0.0)	0 (0.0)	0 (0.0)
TX	6 (1.9)	1 (1.9)	0 (0.0)	0 (0.0)	0 (0.0)

cN stage (%)					
N0	281 (89.2)	50 (96.2)	47 (95.9)	19 (79.2)	18 (72.0)
N1	28 (8.9)	2 (3.8)	2 (4.1)	5 (20.8)	7 (28.0)
NX	6 (1.9)	0 (0.0)	0 (0.0)	0 (0.0)	0 (0.0)
HR tier (%)					
1	21 (9.9)	6 (11.5)	5 (10.0)	3 (12.5)	1 (4.2)
2	58 (27.2)	19 (36.5)	17 (34.0)	5 (20.8)	4 (16.7)
3	103 (48.4)	25 (48.1)	25 (50.0)	11 (45.8)	11 (45.8)
4	31 (14.6)	2 (3.8)	3 (6.0)	5 (20.8)	8 (33.3)
Tempus xT = Yes (%)	281 (87.3)	52 (100.0)	50 (100.0)	24 (100.0)	25 (100.0)
Tempus RNA-seq = Yes (%)	210 (65.2)	36 (69.2)	32 (64.0)	18 (75.0)	21 (84.0)

Table 1. Baseline clinical and pathologic characteristics. Data are presented as n (%) unless otherwise indicated; percentages are proportions of available-data cases for each variable. Total sample size in SP-1 was greater than the planned 45 participants per arm, in part due to operational over-accrual due to time lag between enrollment and SP assignment, and to accommodate potential for non-evaluable participants. Abbreviations: SD, standard deviation; PSA, prostate-specific antigen; IDC, intraductal carcinoma; HR, high risk. “Cribriform” means non-IDC cribriform pattern. The “Overall” column reflects 322 participants enrolled across all GUNS SPs as of July 2026. Of the 322 participants in the “Overall” column, at the time of writing, IDC status was recorded for 201/322, non-IDC cribriform status for 199/322, and HR tier for 213/322; cN stage was not reported for 7/322 in addition to the 6 NX cases.

Supplemental Table S1. Cases meeting GUNS composite MPR but not PROTEUS MRD definition

Cohort	Residual tumour dimensions (mm)	Tumour cellularity	RCB (mm^2)	Pathologic stage / nodal finding	Reason not classified as MRD by PROTEUS
SP1A	2 × 1	0.5%	0.01	ypT3b	ypT3b disease
SP1A	8.8 × 5.8	1%	0.51	ypT2	Largest residual focus > 5 mm
SP1A	7 × 0.3; 1.8 × 1.3	1%; 20%	0.49	ypT3b	ypT3b; largest residual focus > 5 mm
SP1A	11 × 0.48*; 1.6 × 0.76	1%; 3%	0.20	ypT2	Largest residual focus > 5 mm
SP1B	15 × 0.8	3%	0.36	ypT3a	ypT3a; largest residual focus > 5 mm
SP1B	6 × 1.7; 5.4 × 1.4	3%; 1%	0.38	ypT2	Largest residual focus > 5 mm
SP1B	11 × 3.5; 12.4 × 2.7	1%; 1%	0.72	ypT3a; sparse ypN1	Largest residual focus > 5 mm; ypN1
SP1B	11 × 3.8	1%	0.42	ypT2	Largest residual focus > 5 mm
SP1B	11.2 × 7	1%	0.77	ypT3b	ypT3b; largest residual focus > 5 mm
SP1B	6 × 3	1%	0.18	ypT2	Largest residual focus > 5 mm
SP1B	8 × 3	3%	0.77	ypT3b	ypT3b; largest residual focus > 5 mm
SP1B	10 × 2; 6.7 × 1.2	1%; 1%	0.30	ypT2	Largest residual focus > 5 mm
SP1B	5.3 × 2.8	3%	0.74	Focal ypT3a	ypT3a; largest residual focus > 5 mm
SP1B	6 × 0.4	0.1%	0.008	ypT2	Largest residual focus > 5 mm
SP1B	7.4 × 2.1	3%	0.47	ypT2	Largest residual focus > 5 mm
SP1B	7.8 × 1.6	1%	0.12	ypT2	Largest residual focus > 5 mm
SP1B	7.6 × 4.5	1%	1.0	ypT2	Largest residual focus > 5 mm
SP1B	12.2 × 2.8	1%	0.34	Focal ypT3a	ypT3a; largest residual focus > 5 mm
SP1B	11.5 × 1.3	1%	0.15	ypT2	Largest residual focus > 5 mm
SP2B	1.85 × 1.2	70%	1.55	ypT2, sparse ypN1	ypN1 residual disease
SP2B	9.3 × 0.7	1%	0.065	ypT2	Largest residual focus > 5 mm

MRD, minimal residual disease; RCB, residual cancer burden; TC, tumour cellularity. GUNS RCB is calculated as the cumulative residual tumour area (length × width, mm^2) weighted by the corresponding tumour cellularity. The table lists cases classified as MPR by the GUNS composite endpoint but not by the PROTEUS pathologic MRD criteria; each row corresponds to an individual patient. Reasons for discordance are summarized from the case-level information provided. * This 11-mm focus was admixed with histiocytes.

Supplementary Table S2. Treatment-Emergent Serious Adverse Events

Serious adverse event	SP-1A n=52	SP-1B n=50	SP-2A n=24	SP-2B n=25	Total
Patients with ≥1 recorded SAE	**3**	**4**	**1**	**8**	**16**
Infections					
Febrile neutropenia	0	0	0	4	4
Pneumonia	0	1	0	0	1
Postoperative sepsis	0	0	1	0	1
Presacral abscess	1	0	0	0	1
Salmonella infection	1	0	0	0	1
Septic arthritis	0	1	0	0	1
Renal and urinary disorders					
Urinary retention	1	0	0	1	2
Cardiac/vascular disorders					
Coronary artery disease	0	1	0	0	1
Cerebrovascular accident	0	0	0	1	1
Gastrointestinal disorders	0	0	0	1	1
Upper gastrointestinal bleeding	0	0	0	1	1
Metabolism/endocrine					
Hyponatremia/adrenal insufficiency	0	1	0	0	1
Musculoskeletal disorders					
Lower back pain	0	0	0	1	1
Neoplasms					
Neoplasm (see source log)	0	0	0	1	1
General disorders					
Fever	0	0	0	2	2

Treatment-emergent serious adverse events (TE-SAEs) were defined as events occurring from first study treatment until 30 days after completion of protocol therapy. Patients experiencing more than one SAE are counted once in the summary row ("Patients with ≥ 1 TE-SAE") but may contribute to multiple preferred-term categories. Adverse events are grouped according to MedDRA preferred terms.

References

1. National Cancer Institute. Cancer Stat Facts: Prostate Cancer. https://seer.cancer.gov/statfacts/html/prost.html (2026).

2. Cooperberg, M. R., Broering, J. M. & Carroll, P. R. Time trends and local variation in primary treatment of localized prostate cancer. *J. Clin. Oncol.* **28**, 1117–1123 (2010).

3. Wani, M. & Madaan, S. What Is New in the Management of High-Risk Localized Prostate Cancer? *J. Clin. Med.* **12**, 455 (2023).

4. Soloway, M. S. *et al*. Randomized prospective study comparing radical prostatectomy alone versus radical prostatectomy preceded by androgen blockade in clinical stage B2 (T2bNxM0) prostate cancer. The Lupron Depot Neoadjuvant Prostate Cancer Study Group. *J. Urol.* **154**, 424–428 (1995).

5. Klotz, L. H. *et al*. Long-term followup of a randomized trial of 0 versus 3 months of neoadjuvant androgen ablation before radical prostatectomy. *J. Urol.* **170**, 791–794 (2003).

6. Gleave, M. E. *et al*. Randomized comparative study of 3 versus 8-month neoadjuvant hormonal therapy before radical prostatectomy: biochemical and pathological effects. *J. Urol.* **166**, 500–506 (2001).

7. Kyriakopoulos, C. E. *et al*. Chemohormonal Therapy in Metastatic Hormone-Sensitive Prostate Cancer: Long-Term Survival Analysis of the Randomized Phase III E3805 CHAARTED Trial. *J. Clin. Oncol.* **36**, 1080–1087 (2018).

8. James, N. D. *et al*. Addition of docetaxel, zoledronic acid, or both to first-line long-term hormone therapy in prostate cancer (STAMPEDE): survival results from an adaptive, multiarm, multistage, platform randomised controlled trial. *Lancet* **387**, 1163–1177 (2016).

9. James, N. D. *et al*. Abiraterone for Prostate Cancer Not Previously Treated with Hormone Therapy. *N. Engl. J. Med.* **377**, 338–351 (2017).

10. Fizazi, K. *et al*. Abiraterone acetate plus prednisone in patients with newly diagnosed high-risk metastatic castration-sensitive prostate cancer (LATITUDE): final overall survival analysis of a randomised, double-blind, phase 3 trial. *Lancet Oncol.* **20**, 686–700 (2019).

11. Chi, K. N. *et al*. Apalutamide for Metastatic, Castration-Sensitive Prostate Cancer. *N. Engl. J. Med.* **381**, 13–24 (2019).

12. Fizazi, K. *et al*. Abiraterone plus prednisone added to androgen deprivation therapy and docetaxel in de novo metastatic castration-sensitive prostate cancer (PEACE-1): a multicentre, open-label, randomised, phase 3 study with a 2 × 2 factorial design. *Lancet* **399**, 1695–1707 (2022).

13. Smith, M. R. *et al*. Darolutamide and Survival in Metastatic, Hormone-Sensitive Prostate Cancer. *N. Engl. J. Med.* **386**, 1132–1142 (2022).

14. Taplin, M. E. *et al*. Intense androgen-deprivation therapy with abiraterone acetate plus leuprolide acetate in patients with localized high-risk prostate cancer: results of a randomized phase II neoadjuvant study. *J. Clin. Oncol.* **32**, 3705–3715 (2014).

15. Montgomery, B. *et al*. Neoadjuvant Enzalutamide Prior to Prostatectomy. *Clin. Cancer Res.* **23**, 2169–2176 (2017).

16. McKay, R. R. *et al*. Evaluation of Intense Androgen Deprivation Before Prostatectomy: A Randomized Phase II Trial of Enzalutamide and Leuprolide With or Without Abiraterone. *J. Clin. Oncol.* **37**, 923–931 (2019).

17. McKay, R. R. *et al*. Results of a Randomized Phase II Trial of Intense Androgen Deprivation Therapy prior to Radical Prostatectomy in Men with High-Risk Localized Prostate Cancer. *J. Urol.* **206**, 80–87 (2021).

18. Yanagisawa, T. *et al*. Neoadjuvant Androgen Receptor Signaling Inhibitors before Radical Prostatectomy for Non-Metastatic Advanced Prostate Cancer: A Systematic Review. *J. Pers. Med.* **13**, 641 (2023).

19. Eastham, J. A. *et al*. Cancer and Leukemia Group B 90203 (Alliance): Radical Prostatectomy With or Without Neoadjuvant Chemohormonal Therapy in Localized, High-Risk Prostate Cancer. *J. Clin. Oncol.* **38**, 3042–3050 (2020).

20. Fleshner, N. E. *et al*. Neoadjuvant Cabazitaxel plus Abiraterone/Leuprolide Acetate in Patients with High-Risk Prostate Cancer: ACDC-RP Phase II Trial. *Clin. Cancer Res.* **29**, 3867–3874 (2023).

21. Cortazar, P. *et al*. Pathological complete response and long-term clinical benefit in breast cancer: the CTNeoBC pooled analysis. *Lancet* **384**, 164–172 (2014).

22. Vulsteke, C. *et al*. Perioperative Enfortumab Vedotin and Pembrolizumab in Bladder Cancer. *N. Engl. J. Med.* **394**, 1257–1269 (2026).

23. Litton, J. K. *et al*. Standardized Definitions for Efficacy End Points in Neoadjuvant Breast Cancer Clinical Trials: NeoSTEEP. *J. Clin. Oncol.* **41**, 4433–4442 (2023).

24. U.S. Food and Drug Administration. Pathological Complete Response in Neoadjuvant Treatment of High-Risk Early-Stage Breast Cancer: Use as an Endpoint to Support Accelerated Approval. Guidance for Industry, Docket No. FDA-2012-D-0432 (FDA, 2020).

25. Taplin, M. E. *et al*. Perioperative Apalutamide in High-Risk Localized Prostate Cancer. *N. Engl. J. Med.* **395**, 546–560 (2026).

26. Cancer Genome Atlas Research Network. The Molecular Taxonomy of Primary Prostate Cancer. *Cell* **163**, 1011–1025 (2015).

27. Wei, L. *et al*. Intratumoral and Intertumoral Genomic Heterogeneity of Multifocal Localized Prostate Cancer Impacts Molecular Classifications and Genomic Prognosticators. *Eur. Urol.* **71**, 183–192 (2017).

28. Yamaguchi, T. N. *et al*. The Germline and Somatic Origins of Prostate Cancer Heterogeneity. *Cancer Discov.* **15**, 988–1017 (2025).

29. Attard, G. *et al*. Niraparib and abiraterone acetate plus prednisone for HRR-deficient metastatic castration-sensitive prostate cancer: a randomized phase 3 trial. *Nat. Med.* **31**, 4109–4118 (2025).

30. Agarwal, N. *et al*. PARP and Androgen-Signaling Inhibition plus ADT in Metastatic Prostate Cancer. *N. Engl. J. Med.* **395**, 427–439 (2026).

31. Fizazi, K. *et al*. Capivasertib plus abiraterone in PTEN-deficient metastatic hormone-sensitive prostate cancer: CAPItello-281 phase III study. *Ann. Oncol.* **37**, 53–68 (2026).

689 32. Carver, B. S. *et al*. Aberrant ERG expression cooperates with loss of PTEN to promote cancer
690 progression in the prostate. *Nat. Genet.* **41**, 619–624 (2009).

691 33. King, J. C. *et al*. Cooperativity of *TMPRSS2-ERG* with PI3-kinase pathway activation in prostate
692 oncogenesis. *Nat. Genet.* **41**, 524–526 (2009).

693 34. Leinonen, K. A. *et al*. Loss of PTEN is associated with aggressive behavior in ERG-positive prostate
694 cancer. *Cancer Epidemiol. Biomarkers Prev.* **22**, 2333–2344 (2013).

695 35. Blee, A. M. *et al*. *TMPRSS2-ERG* Controls Luminal Epithelial Lineage and Antiandrogen Sensitivity in
696 *PTEN* and *TP53*-Mutated Prostate Cancer. *Clin. Cancer Res.* **24**, 4551–4565 (2018).

697 36. Nakazawa, M. *et al*. Clinical and genomic features of *SPOP*-mutant prostate cancer. *Prostate* **82**,
698 260–268 (2022).

699 37. Lotan, T. L. *et al*. Cytoplasmic PTEN protein loss distinguishes intraductal carcinoma of the prostate
700 from high-grade prostatic intraepithelial neoplasia. *Mod. Pathol.* **26**, 587–603 (2013).

701 38. Böttcher, R. *et al*. Cribriform and intraductal prostate cancer are associated with increased genomic
702 instability and distinct genomic alterations. *BMC Cancer* **18**, 8 (2018).

703 39. Stopsack, K. H. *et al*. Differences in Prostate Cancer Genomes by Self-reported Race: Contributions of
704 Genetic Ancestry, Modifiable Cancer Risk Factors, and Clinical Factors. *Clin. Cancer Res.* **28**, 318–326
705 (2022).

706 40. Kron, K. J. *et al*. *TMPRSS2-ERG* fusion co-opts master transcription factors and activates NOTCH
707 signaling in primary prostate cancer. *Nat. Genet.* **49**, 1336–1345 (2017).

708 41. Stelloo, S. *et al*. Integrative epigenetic taxonomy of primary prostate cancer. *Nat. Commun.* **9**, 4900
709 (2018).

710 42. You, S. *et al*. Integrated Classification of Prostate Cancer Reveals a Novel Luminal Subtype with Poor
711 Outcome. *Cancer Res.* **76**, 4948–4958 (2016).

712 43. Zhao, S. G. *et al*. Associations of Luminal and Basal Subtyping of Prostate Cancer With Prognosis and
713 Response to Androgen Deprivation Therapy. *JAMA Oncol.* **3**, 1663–1672 (2017).

714 44. Yoon, J. *et al*. A comparative study of PCS and PAM50 prostate cancer classification schemes.
715 *Prostate Cancer Prostatic Dis.* **24**, 733–742 (2021).

716 45. Grist, E. *et al*. Tumor transcriptome-wide expression classifiers predict treatment sensitivity in
717 advanced prostate cancers. *Cell* **188**, 5717–5734.e10 (2025).

718 46. Beaubier, N. *et al*. Clinical validation of the tempus xT next-generation targeted oncology sequencing
719 assay. *Oncotarget* **10**, 2384–2396 (2019).

720 47. McKay, R. R. *et al*. Post prostatectomy outcomes of patients with high-risk prostate cancer treated
721 with neoadjuvant androgen blockade. *Prostate Cancer Prostatic Dis.* **21**, 364–372 (2018).

722 48. Mostaghel, E. A. *et al*. Targeted androgen pathway suppression in localized prostate cancer: a pilot
723 study. *J. Clin. Oncol.* **32**, 229–237 (2014).

724 49. Sumiyoshi, T. *et al*. Molecular features of prostate cancer after neoadjuvant therapy in the phase 3
725 CALGB 90203 trial. *J. Natl Cancer Inst.* **116**, 115–126 (2024).

50. Chi, K. N. *et al*. Multicenter phase II study of combined neoadjuvant docetaxel and hormone therapy before radical prostatectomy for patients with high risk localized prostate cancer. *J. Urol.* **180**, 565–570 (2008).

51. Amiri-Kordestani, L. *et al*. First FDA approval of neoadjuvant therapy for breast cancer: pertuzumab for the treatment of patients with HER2-positive breast cancer. *Clin. Cancer Res.* **20**, 5359–5364 (2014).

52. Petrelli, F. *et al*. Correlation of pathologic complete response with survival after neoadjuvant chemotherapy in bladder cancer treated with cystectomy: a meta-analysis. *Eur. Urol.* **65**, 350–357 (2014).

53. Symmans, W. F. *et al*. Measurement of residual breast cancer burden to predict survival after neoadjuvant chemotherapy. *J. Clin. Oncol.* **25**, 4414–4422 (2007).

54. Pusztai, L. *et al*. Durvalumab with olaparib and paclitaxel for high-risk HER2-negative stage II/III breast cancer: Results from the adaptively randomized I-SPY2 trial. *Cancer Cell* **39**, 989–998.e5 (2021).

55. Rugo, H. S. *et al*. Adaptive Randomization of Veliparib-Carboplatin Treatment in Breast Cancer. *N. Engl. J. Med.* **375**, 23–34 (2016).

56. Ravi, P. *et al*. Long-term Outcomes and Prognostic Impact of Residual Cancer Burden After Intensified Neoadjuvant Therapy in High-risk Prostate Cancer. *Eur. Urol.* **87**, 643–650 (2025).

57. Saad, F. *et al*. Apalutamide plus abiraterone acetate and prednisone versus placebo plus abiraterone and prednisone in metastatic, castration-resistant prostate cancer (ACIS): a randomised, placebo-controlled, double-blind, multinational, phase 3 study. *Lancet Oncol.* **22**, 1541–1559 (2021).

58. Attard, G. *et al*. Abiraterone acetate plus prednisolone with or without enzalutamide for patients with metastatic prostate cancer starting androgen deprivation therapy: final results from two randomised phase 3 trials of the STAMPEDE platform protocol. *Lancet Oncol.* **24**, 443–456 (2023).

59. Annala, M. *et al*. Circulating Tumor DNA Genomics Correlate with Resistance to Abiraterone and Enzalutamide in Prostate Cancer. *Cancer Discov.* **8**, 444–457 (2018).

60. Khalaf, D. J. *et al*. Optimal sequencing of enzalutamide and abiraterone acetate plus prednisone in metastatic castration-resistant prostate cancer: a multicentre, randomised, open-label, phase 2, crossover trial. *Lancet Oncol.* **20**, 1730–1739 (2019).

61. Sekar, A. *et al*. *TMPRSS2-ERG* confers resistance of prostate cancer to antiandrogens. *EMBO Mol. Med.* **18**, 2062–2097 (2026).

62. Liao, Y., Smyth, G. K. & Shi, W. featureCounts: an efficient general purpose program for assigning sequence reads to genomic features. *Bioinformatics* **30**, 923–930 (2014).

63. Love, M. I., Huber, W. & Anders, S. Moderated estimation of fold change and dispersion for RNA-seq data with DESeq2. *Genome Biol.* **15**, 550 (2014).

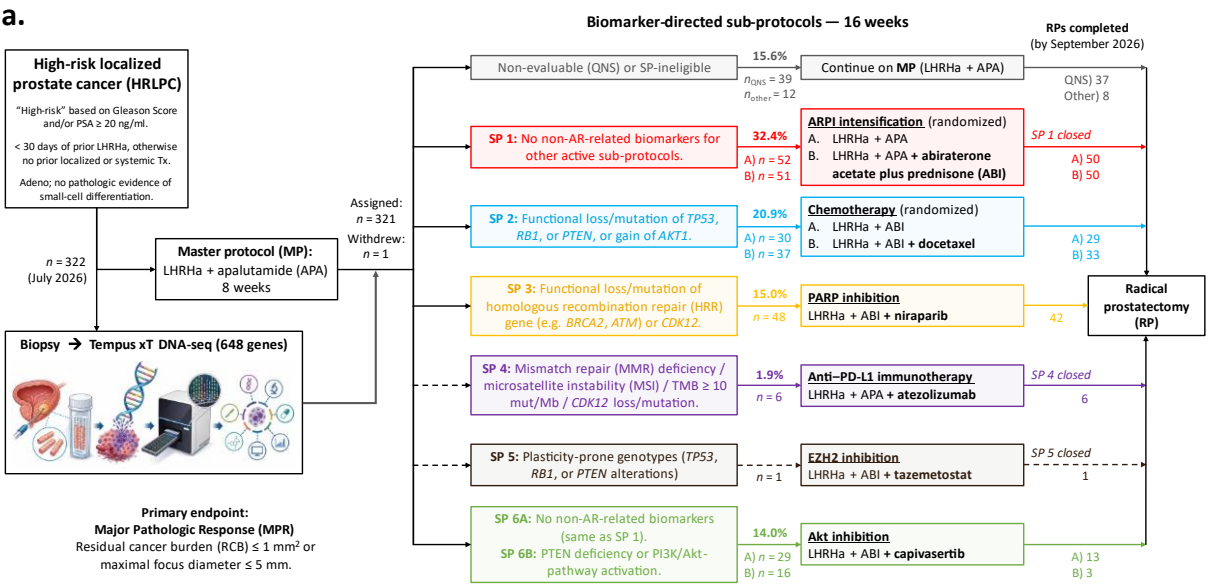
64. Robinson, M. D., McCarthy, D. J. & Smyth, G. K. edgeR: a Bioconductor package for differential expression analysis of digital gene expression data. *Bioinformatics* **26**, 139–140 (2010).

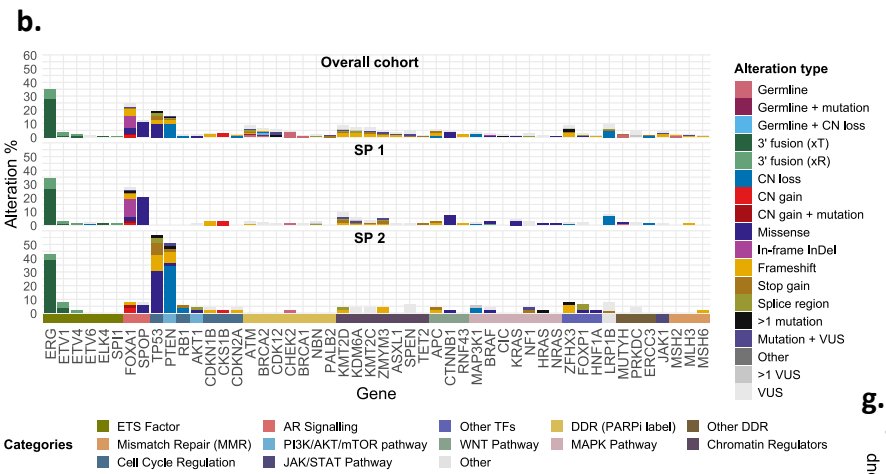
65. Ritchie, M. E. *et al*. limma powers differential expression analyses for RNA-sequencing and microarray studies. *Nucleic Acids Res.* **43**, e47 (2015).

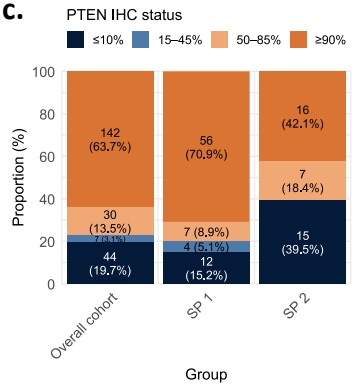
66. Simon, R. Optimal two-stage designs for phase II clinical trials. *Control. Clin. Trials* **10**, 1–10 (1989).

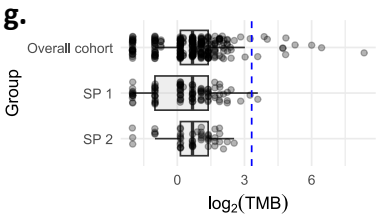
67. Fang, Z., Liu, X. & Peltz, G. GSEApy: a comprehensive package for performing gene set enrichment analysis in Python. *Bioinformatics* **39**, btac757 (2023).

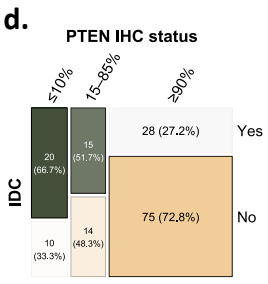
Figure 1.

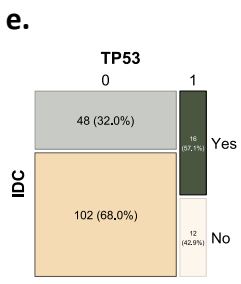

a.
Biomarker-directed sub-protocols — 16 weeks
RPs completed (by September 2026)
High-risk localized prostate cancer (HRLPC)
"High-risk" based on Gleason Score and/or PSA ≥ 20 ng/ml.
< 30 days of prior LHRHa, otherwise no prior localized or systemic Tx.
Adeno; no pathologic evidence of small-cell differentiation.
n = 322 (July 2026)
Master protocol (MP): LHRHa + apalutamide (APA) 8 weeks
Assigned: n = 321
Withdrew: n = 1
Biopsy → Tempus xT DNA-seq (648 genes)
Primary endpoint:
Major Pathologic Response (MPR)
Residual cancer burden (RCB) ≤ 1 mm² or maximal focus diameter ≤ 5 mm.
Non-evaluable (QNS) or SP-ineligible
15.6%
n_QNS = 39
n_other = 12
Continue on MP (LHRHa + APA)
QNS) 37
Other) 8
SP 1: No non-AR-related biomarkers for other active sub-protocols.
32.4%
A) n = 52
B) n = 51
ARPI intensification (randomized)
A. LHRHa + APA
B. LHRHa + APA + abiraterone acetate plus prednisone (ABI)
SP 1 closed
A) 50
B) 50
SP 2: Functional loss/mutation of TP53, RB1, or PTEN, or gain of AKT1.
20.9%
A) n = 30
B) n = 37
Chemotherapy (randomized)
A. LHRHa + ABI
B. LHRHa + ABI + docetaxel
A) 29
B) 33
SP 3: Functional loss/mutation of homologous recombination repair (HRR) gene (e.g. BRCA2, ATM) or CDK12.
15.0%
n = 48
PARP inhibition
LHRHa + ABI + niraparib
42
Radical prostatectomy (RP)
SP 4: Mismatch repair (MMR) deficiency / microsatellite instability (MSI) / TMB ≥ 10 mut/Mb / CDK12 loss/mutation.
1.9%
n = 6
Anti–PD-L1 immunotherapy
LHRHa + APA + atezolizumab
SP 4 closed
6
SP 5: Plasticity-prone genotypes (TP53, RB1, or PTEN alterations)
n = 1
EZH2 inhibition
LHRHa + ABI + tazemetostat
SP 5 closed
1
SP 6A: No non-AR-related biomarkers (same as SP 1).
SP 6B: PTEN deficiency or PI3K/Akt-pathway activation.
14.0%
A) n = 29
B) n = 16
Akt inhibition
LHRHa + ABI + capivasertib
A) 13
B) 3

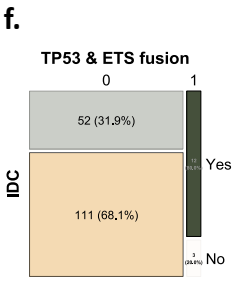

b.
Overall cohort
SP 1
SP 2
Alteration %
Gene
Alteration type
Germline
Germline + mutation
Germline + CN loss
3' fusion (xT)
3' fusion (xR)
CN loss
CN gain
CN gain + mutation
Missense
In-frame InDel
Frameshift
Stop gain
Splice region
>1 mutation
Mutation + VUS
Other
>1 VUS
VUS
Categories
ETS Factor
Mismatch Repair (MMR)
Cell Cycle Regulation
AR Signalling
PI3K/AKT/mTOR pathway
JAK/STAT Pathway
Other TFs
WNT Pathway
Other
DDR (PARPi label)
MAPK Pathway
Other DDR
Chromatin Regulators


c.
PTEN IHC status
≤10%
15–45%
50–85%
≥90%
Proportion (%)
142 (63.7%)
30 (13.5%)
7 (3.1%)
44 (19.7%)
56 (70.9%)
7 (8.9%)
4 (5.1%)
12 (15.2%)
16 (42.1%)
7 (18.4%)
15 (39.5%)
Overall cohort
SP 1
SP 2
Group


g.
Overall cohort
SP 1
SP 2
Group
log2(TMB)


d.
PTEN IHC status
≤10%
15–85%
≥90%
IDC
20 (66.7%)
15 (51.7%)
10 (33.3%)
14 (48.3%)
28 (27.2%)
75 (72.8%)
Yes
No
Pearson χ² (two-sided)
X² = 17.7
P two-sided < 0.001


e.
TP53
0
1
IDC
48 (32.0%)
102 (68.0%)
16 (57.1%)
12 (42.9%)
Yes
No
Pearson χ² (two-sided)
X² = 6.48
P two-sided = 0.0109


f.
TP53 & ETS fusion
0
1
IDC
52 (31.9%)
111 (68.1%)
Yes
No
Pearson χ² (two-sided)
X² = 13.8
P two-sided < 0.001

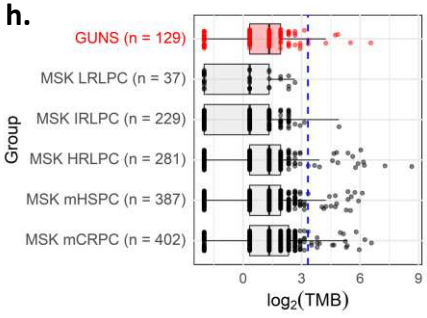

h.
GUNS (n = 129)
MSK LRLPC (n = 37)
MSK IRLPC (n = 229)
MSK HRLPC (n = 281)
MSK mHSPC (n = 387)
MSK mCRPC (n = 402)
Group
log2(TMB)

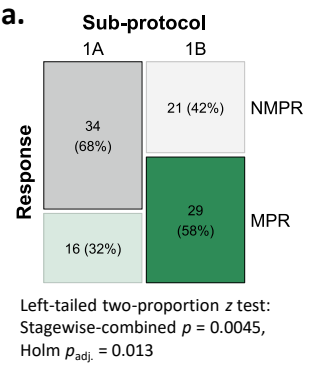
Figure 2.

SP-1: AR-associated genomics / no biomarkers for other SPs.

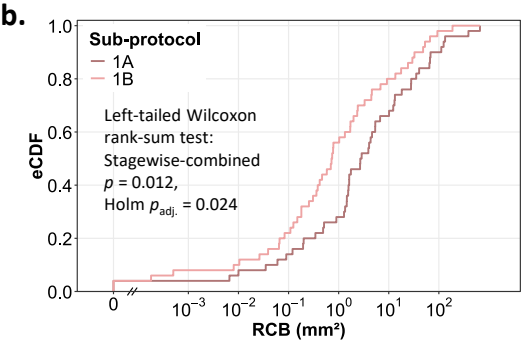
SP-1A: LHRHa + APA
SP-1B: LHRHa + APA + ABI

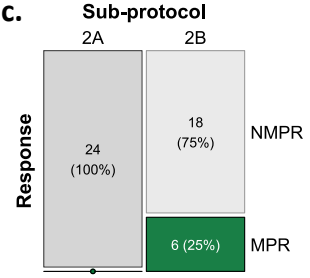
SP-2: *TP53*^{alt}, *PTEN*^{alt}/*AKT1*^{GOF}, or *RB1*^{alt}.

SP-2A: LHRHa + ABI
SP-2B: LHRHa + ABI + docetaxel

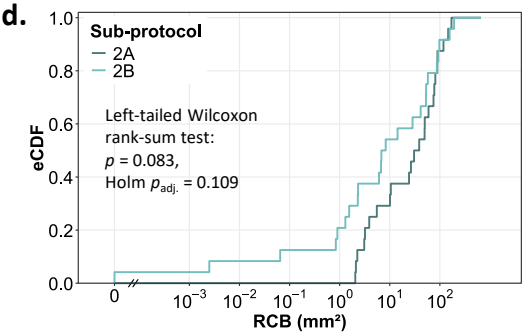


Left-tailed two-proportion z test: Stagewise-combined p = 0.0045, Holm $p_{adj.}$ = 0.013





Left-tailed Fisher's exact test: p = 0.011, Holm $p_{adj.}$ = 0.033



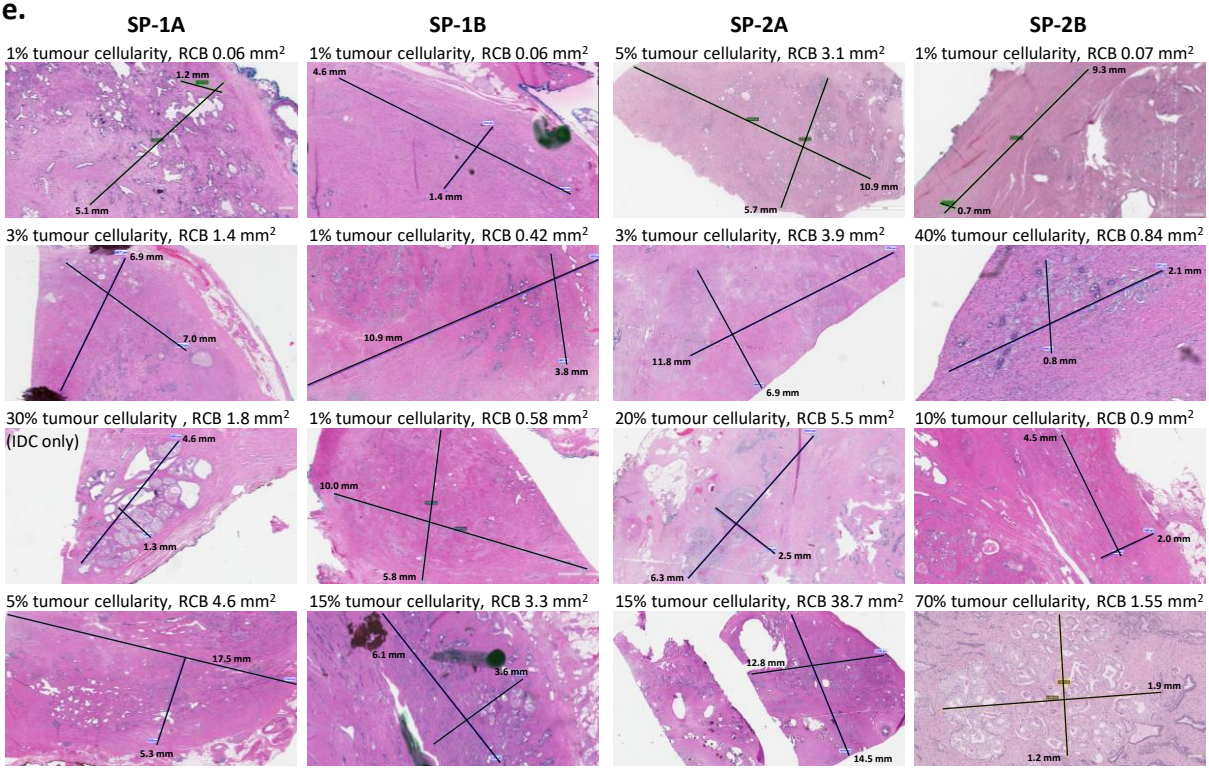
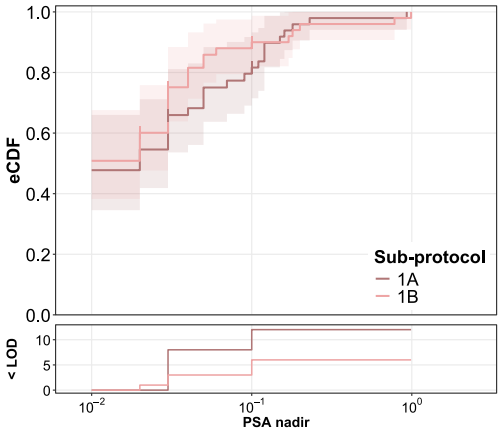


Figure 3.

SP-1: AR-associated genomics / no biomarkers for other SPs.

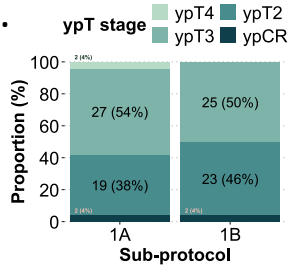
SP-1A: LHRHa + APA
SP-1B: LHRHa + APA + ABI

a.



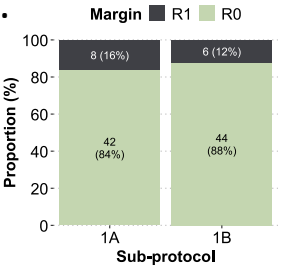
Reverse-KM log-rank (left-tailed)
z = -0.617
$p_{left} = 0.269$

b.



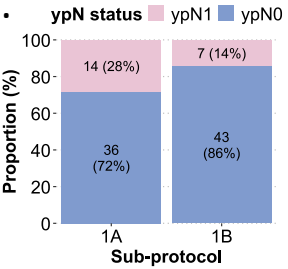
Kendall tau-b (left-tailed)
$\tau_b = -0.0922$
$p_{left} = 0.173$

c.



One-sided two-proportion z-test (no continuity correction) (left-tailed)
z = -0.576
$p_{left} = 0.282$

d.

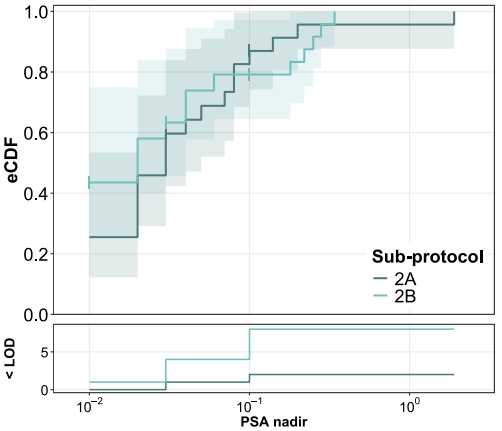


One-sided two-proportion z-test (no continuity correction) (left-tailed)
z = -1.72
$p_{left} = 0.0428$

SP-2: *TP53*^{alt}, *PTEN*^{alt}/*AKT1*^{GOF}, or *RB1*^{alt}.

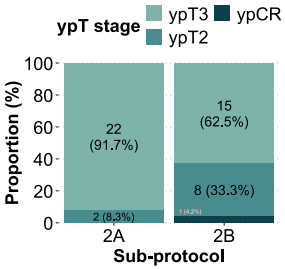
SP-2A: LHRHa + ABI
SP-2B: LHRHa + ABI + docetaxel

e.



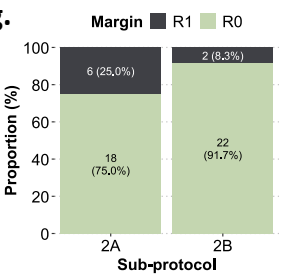
Reverse-KM log-rank (left-tailed)
z = -1.01
$p_{left} = 0.157$

f.



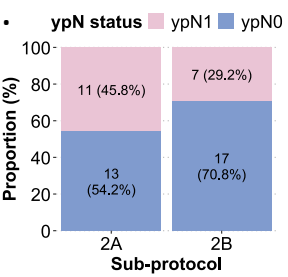
Kendall tau-b (left-tailed)
$\tau_b = -0.347$
$p_{left} = 0.00819$

g.



Fisher exact (one-sided) (left-tailed)
log(OR) = -1.27
$p_{left} = 0.122$

h.



One-sided two-proportion z-test (no continuity correction) (left-tailed)
z = -1.19
$p_{left} = 0.117$

Figure 4.

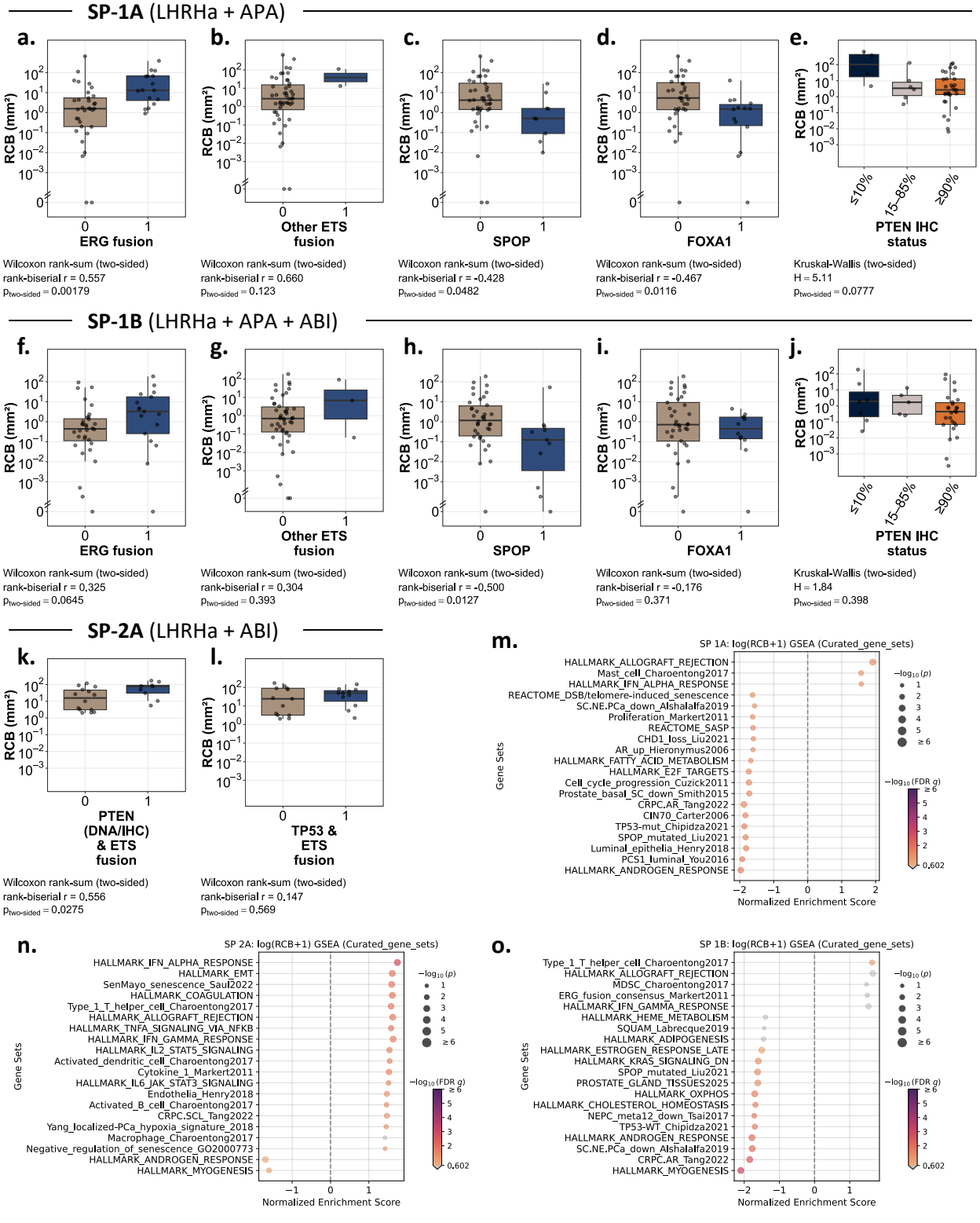
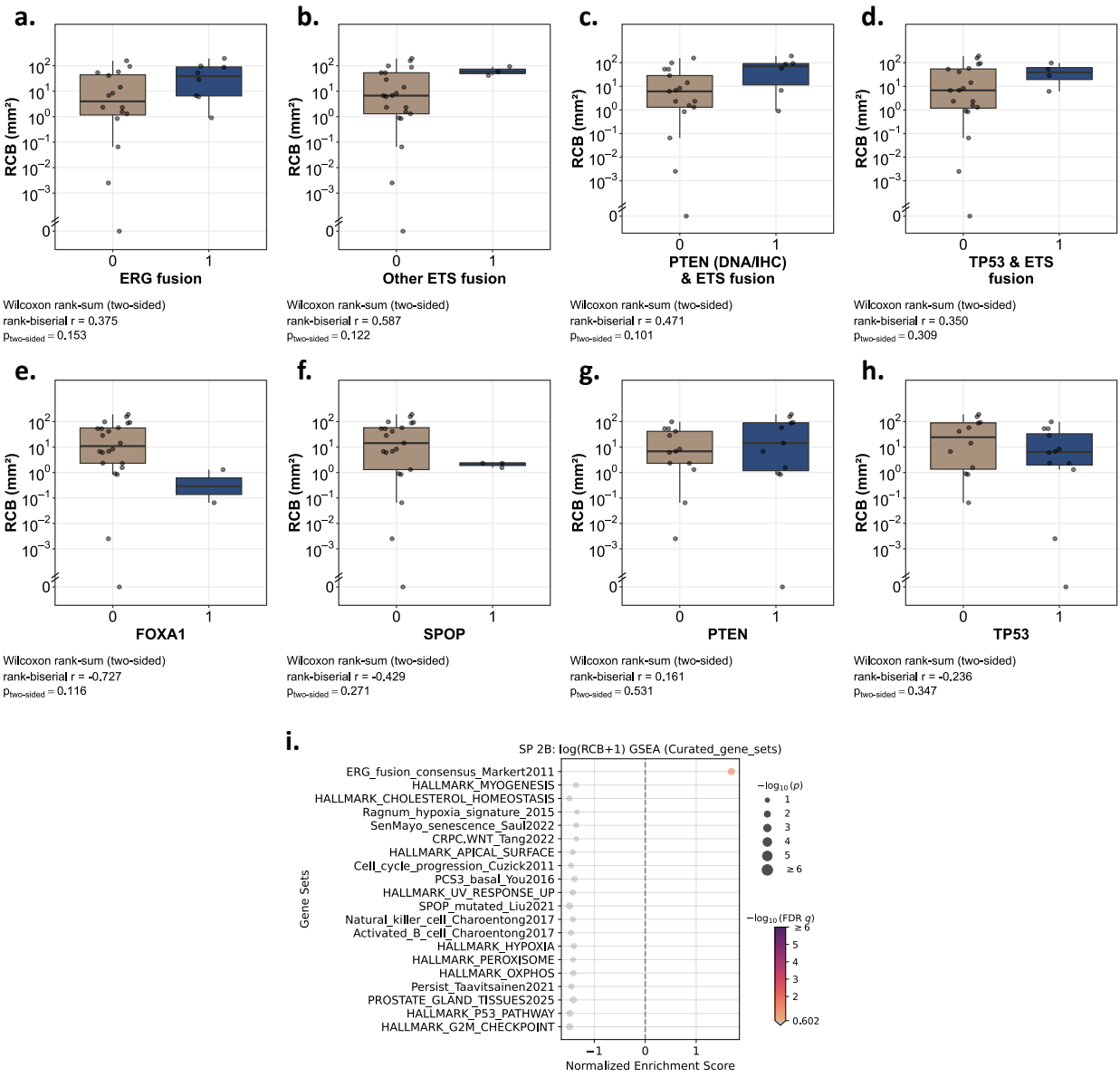
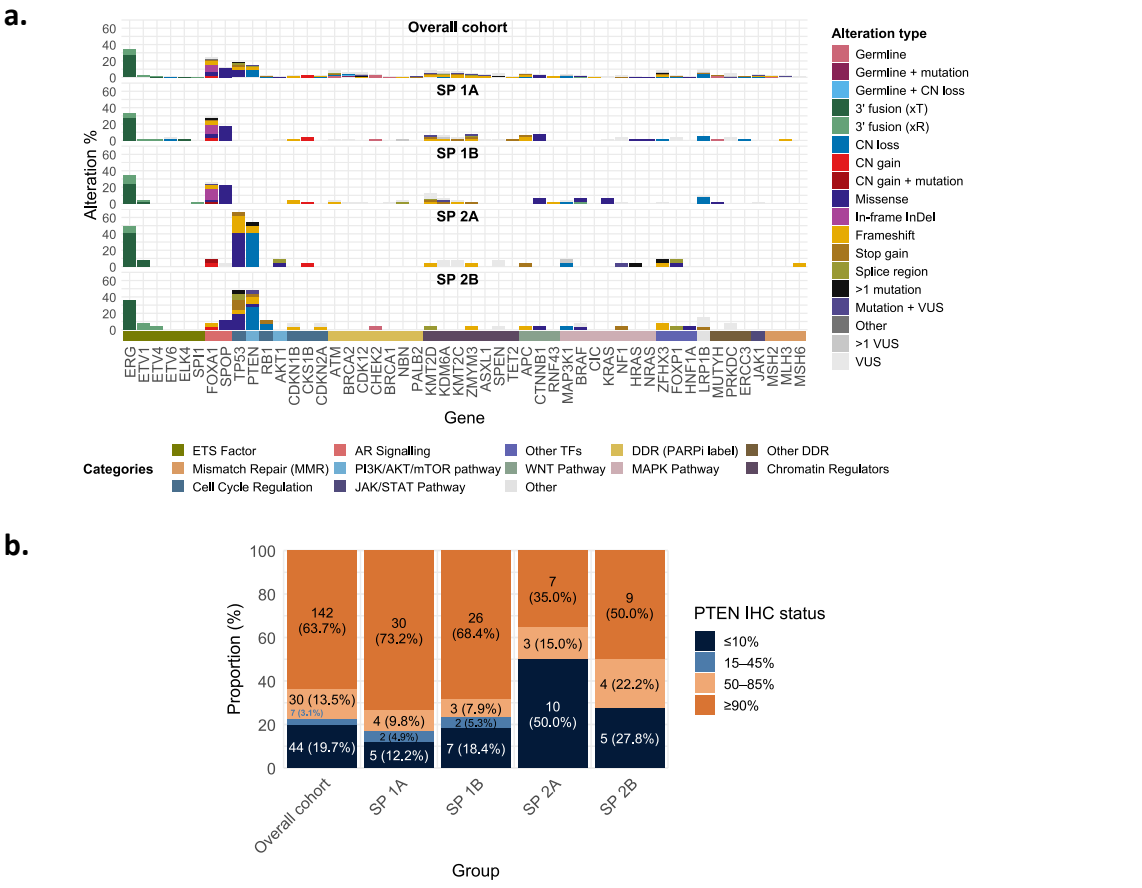

SP-1A (LHRHa + APA)
a.
RCB (mm²)
ERG fusion
Wilcoxon rank-sum (two-sided)
rank-biserial r = 0.557
p two-sided = 0.00179
b.
Other ETS fusion
Wilcoxon rank-sum (two-sided)
rank-biserial r = 0.660
p two-sided = 0.123
c.
SPOP
Wilcoxon rank-sum (two-sided)
rank-biserial r = -0.428
p two-sided = 0.0482
d.
FOXA1
Wilcoxon rank-sum (two-sided)
rank-biserial r = -0.467
p two-sided = 0.0116
e.
≤10%
15–85%
≥90%
PTEN IHC status
Kruskal-Wallis (two-sided)
H = 5.11
p two-sided = 0.0777
SP-1B (LHRHa + APA + ABI)
f.
ERG fusion
Wilcoxon rank-sum (two-sided)
rank-biserial r = 0.325
p two-sided = 0.0645
g.
Other ETS fusion
Wilcoxon rank-sum (two-sided)
rank-biserial r = 0.304
p two-sided = 0.393
h.
SPOP
Wilcoxon rank-sum (two-sided)
rank-biserial r = -0.500
p two-sided = 0.0127
i.
FOXA1
Wilcoxon rank-sum (two-sided)
rank-biserial r = -0.176
p two-sided = 0.371
j.
≤10%
15–85%
≥90%
PTEN IHC status
Kruskal-Wallis (two-sided)
H = 1.84
p two-sided = 0.398
SP-2A (LHRHa + ABI)
k.
PTEN (DNA/IHC) & ETS fusion
Wilcoxon rank-sum (two-sided)
rank-biserial r = 0.556
p two-sided = 0.0275
l.
TP53 & ETS fusion
Wilcoxon rank-sum (two-sided)
rank-biserial r = 0.147
p two-sided = 0.569
m.
SP 1A: log(RCB+1) GSEA (Curated_gene_sets)
HALLMARK_ALLOGRAFT_REJECTION
Mast_cell_Charoentong2017
HALLMARK_IFN_ALPHA_RESPONSE
REACTOME_DSB/telomere-induced_senescence
SC.NE.PCa_down_Alshalalfa2019
Proliferation_Markert2011
REACTOME_SASP
CHD1_loss_Liu2021
AR_up_Hieronymus2006
HALLMARK_FATTY_ACID_METABOLISM
HALLMARK_E2F_TARGETS
Cell_cycle_progression_Cuzick2011
Prostate_basal_SC_down_Smith2015
CRPC.AR_Tang2022
CIN70_Carter2006
TP53-mut_Chipidza2021
SPOP_mutated_Liu2021
Luminal_epithelia_Henry2018
PCS1_luminal_You2016
HALLMARK_ANDROGEN_RESPONSE
Gene Sets
Normalized Enrichment Score
n.
SP 2A: log(RCB+1) GSEA (Curated_gene_sets)
HALLMARK_IFN_ALPHA_RESPONSE
HALLMARK_EMT
SenMayo_senescence_Saul2022
HALLMARK_COAGULATION
Type_1_T_helper_cell_Charoentong2017
HALLMARK_ALLOGRAFT_REJECTION
HALLMARK_TNFA_SIGNALING_VIA_NFKB
HALLMARK_IFN_GAMMA_RESPONSE
HALLMARK_IL2_STAT5_SIGNALING
Activated_dendritic_cell_Charoentong2017
Cytokine_1_Markert2011
HALLMARK_IL6_JAK_STAT3_SIGNALING
Endothelia_Henry2018
Activated_B_cell_Charoentong2017
CRPC.SCL_Tang2022
Yang_localized-PCa_hypoxia_signature_2018
Macrophage_Charoentong2017
Negative_regulation_of_senescence_GO2000773
HALLMARK_ANDROGEN_RESPONSE
HALLMARK_MYOGENESIS
Gene Sets
Normalized Enrichment Score
o.
SP 1B: log(RCB+1) GSEA (Curated_gene_sets)
Type_1_T_helper_cell_Charoentong2017
HALLMARK_ALLOGRAFT_REJECTION
MDSC_Charoentong2017
ERG_fusion_consensus_Markert2011
HALLMARK_IFN_GAMMA_RESPONSE
HALLMARK_HEME_METABOLISM
SQUAM_Labrecque2019
HALLMARK_ADIPOGENESIS
HALLMARK_ESTROGEN_RESPONSE_LATE
HALLMARK_KRAS_SIGNALING_DN
SPOP_mutated_Liu2021
PROSTATE_GLAND_TISSUES2025
HALLMARK_OXPHOS
HALLMARK_CHOLESTEROL_HOMEOSTASIS
NEPC_meta12_down_Tsai2017
TP53-WT_Chipidza2021
HALLMARK_ANDROGEN_RESPONSE
SC.NE.PCa_down_Alshalalfa2019
CRPC.AR_Tang2022
HALLMARK_MYOGENESIS
Gene Sets
Normalized Enrichment Score

Figure 5.


a.
RCB (mm²)
ERG fusion
Wilcoxon rank-sum (two-sided)
rank-biserial r = 0.375
p two-sided = 0.153
b.
RCB (mm²)
Other ETS fusion
Wilcoxon rank-sum (two-sided)
rank-biserial r = 0.587
p two-sided = 0.122
c.
RCB (mm²)
PTEN (DNA/IHC) & ETS fusion
Wilcoxon rank-sum (two-sided)
rank-biserial r = 0.471
p two-sided = 0.101
d.
RCB (mm²)
TP53 & ETS fusion
Wilcoxon rank-sum (two-sided)
rank-biserial r = 0.350
p two-sided = 0.309
e.
RCB (mm²)
FOXA1
Wilcoxon rank-sum (two-sided)
rank-biserial r = -0.727
p two-sided = 0.116
f.
RCB (mm²)
SPOP
Wilcoxon rank-sum (two-sided)
rank-biserial r = -0.429
p two-sided = 0.271
g.
RCB (mm²)
PTEN
Wilcoxon rank-sum (two-sided)
rank-biserial r = 0.161
p two-sided = 0.531
h.
RCB (mm²)
TP53
Wilcoxon rank-sum (two-sided)
rank-biserial r = -0.236
p two-sided = 0.347
i.
SP 2B: log(RCB+1) GSEA (Curated_gene_sets)
Gene Sets
ERG_fusion_consensus_Markert2011
HALLMARK_MYOGENESIS
HALLMARK_CHOLESTEROL_HOMEOSTASIS
Ragnum_hypoxia_signature_2015
SenMayo_senescence_Saul2022
CRPC.WNT_Tang2022
HALLMARK_APICAL_SURFACE
Cell_cycle_progression_Cuzick2011
PCS3_basal_You2016
HALLMARK_UV_RESPONSE_UP
SPOP_mutated_Liu2021
Natural_killer_cell_Charoentong2017
Activated_B_cell_Charoentong2017
HALLMARK_HYPOXIA
HALLMARK_PEROXISOME
HALLMARK_OXPHOS
Persist_Taavitsainen2021
PROSTATE_GLAND_TISSUES2025
HALLMARK_P53_PATHWAY
HALLMARK_G2M_CHECKPOINT
−log10 (p)
−log10 (FDR q)
0.602
Normalized Enrichment Score

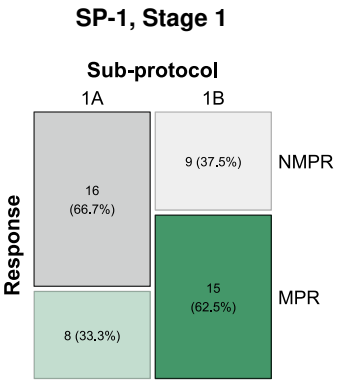
Supplementary Figures

Supplementary Figure S1.

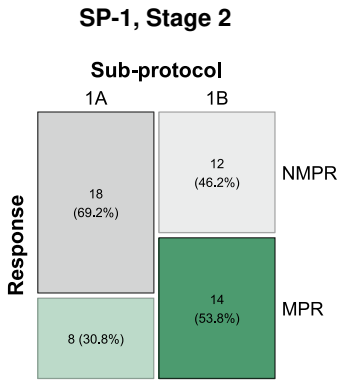


Supplementary Figure S2.

a.

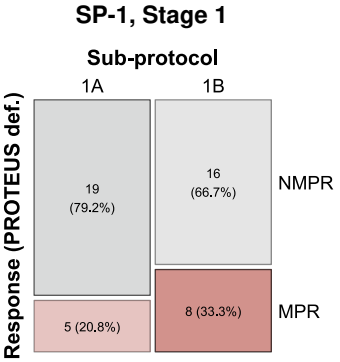


One-sided two-proportion z-test (no continuity correction)
(left-tailed)
z = -2.02
$p_{left} = 0.0216$

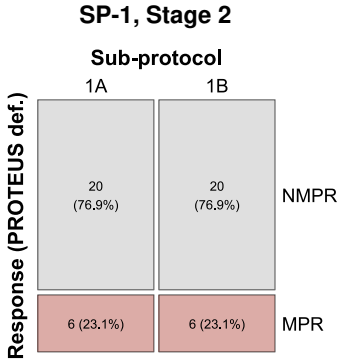


One-sided two-proportion z-test (no continuity correction)
(left-tailed)
z = -1.68
$p_{left} = 0.0461$

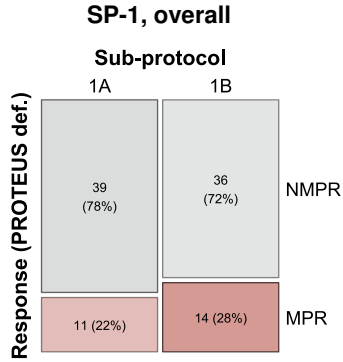
b.



One-sided two-proportion z-test (no continuity correction)
(left-tailed)
z = -0.974
$p_{left} = 0.165$

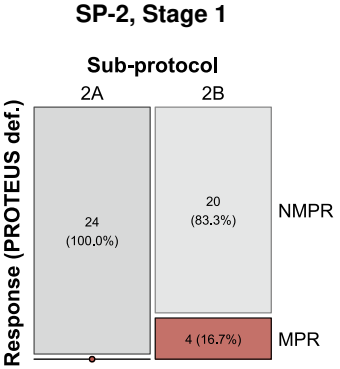


One-sided two-proportion z-test (no continuity correction)
(left-tailed)
z = 0
$p_{left} = 0.5$



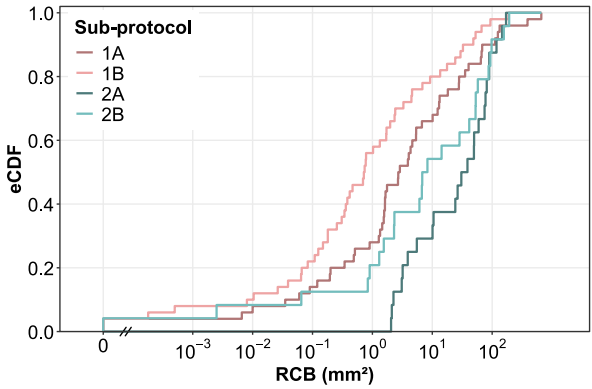
One-sided two-proportion z-test (no continuity correction)
(left-tailed)
z = -0.693
$p_{left} = 0.244$

c.



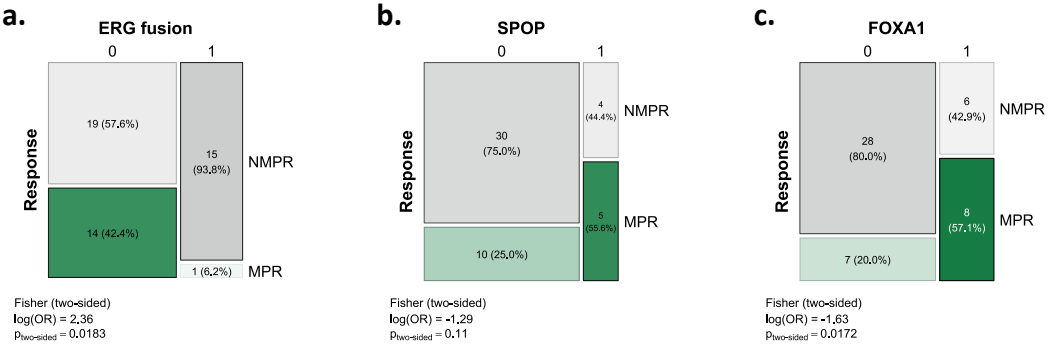
Fisher exact (one-sided) (left-tailed)
log(OR) = -Inf
$p_{left} = 0.0546$

d.

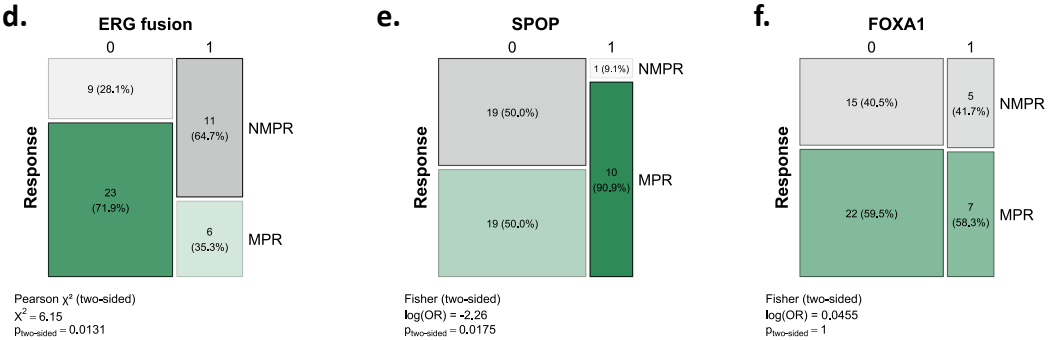


Supplementary Figure S3.

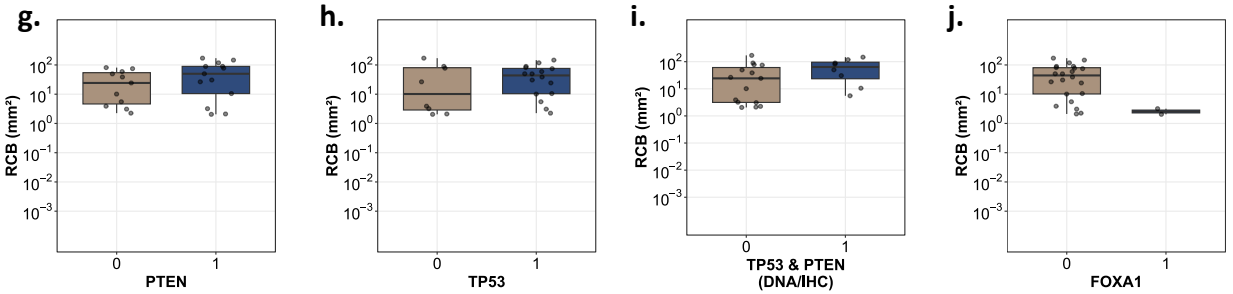
SP-1A



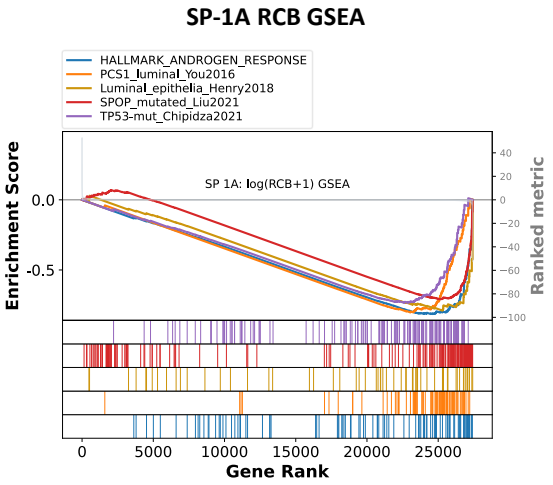
SP-1B

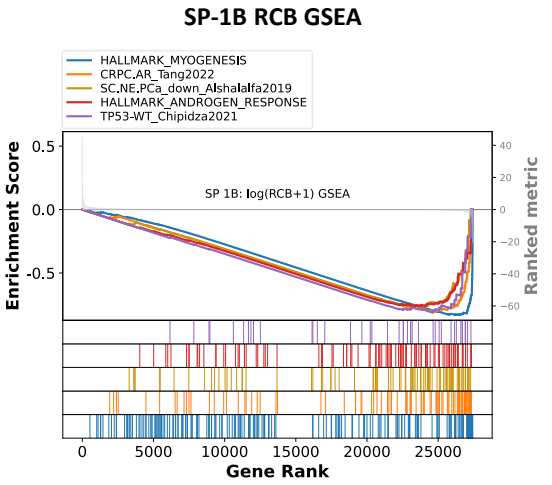


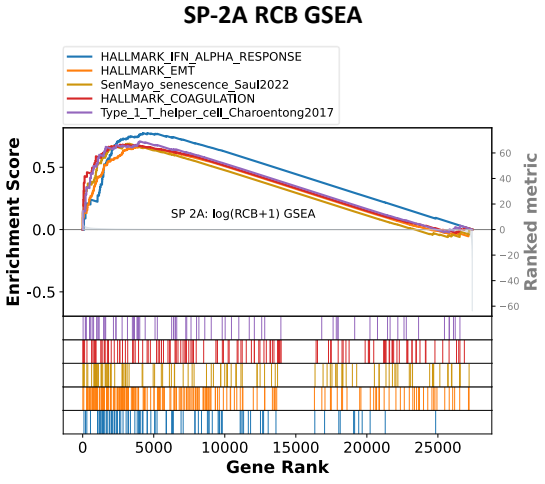
SP-2A



Supplementary Figure S4.







Supplementary Files

This is a list of supplementary files associated with this preprint. Click to download.

- 171curatedgenesetsforPCaGSEA.ENSG.txt
- 171curatedgenesetsforPCaGSEA.symbols.txt
- GleaveetalGUNSNatureMedSupplement.docx